 doi:10.20944/preprints202210.0388.v1

Review

Iridium-based Electrocatalysts for Acidic Oxygen Evolution Reaction: Engineering Strategies to Enhance the Activity and Stability

Hongzhe Xu[1,2], Yun Han[1,2], Qin Li[1,2*] and Xuecheng Yan[1*]

[1] Queensland Micro- and Nanotechnology Centre, Griffith University, Nathan Campus, QLD 4111, Australia
[2] School of Engineering and Built Environment, Griffith University, Nathan Campus, QLD 4111, Australia
*Corresponding author: qin.li@griffith.edu.au (Q. Li), x.yan@griffith.edu.au (X. Yan)

Abstract: Proton exchange membrane water electrolyzers (PEMWEs) for water electrolysis have received tremendous attention due to their immediate response, high proton conductivity, low ohmic losses and gas crossover rate. However, design high activity, economical and long-term durable electrocatalysts in an acidic environment is still the bottleneck to realize the large-scale commercialization of PEMWEs. Iridium-based materials represent one of the most promising classes of oxygen evolution reaction (OER) catalysts due to their intrinsic stability in acid media over ruthenium-based counterparts. However, only a few innovative approaches have been developed to synthesizing iridium-based catalysts (IBCs) in the past decade, mainly due to achieving high activity may deteriorate the stability of IBCs. Accordingly, various engineering strategies of optimizing IBCs have been proposed to address this issue, including doping engineering, morphology engineering, crystal phase engineering and support engineering. Herein, a critical overview focusing on various synthesis and modulation strategies of IBCs is presented, based on an in-depth understanding of the relationship between electronic structures, charge redistribution and activity as well as stability of the electrocatalysts. In addition, the unprecedented achievements in PEMWEs are summarized. The reaction mechanisms and future perspectives are critically discussed to inspire more rational design of IBCs toward practical applications.

Keywords: oxygen evolution reaction; water electrolysis; iridium-based catalysts; engineering strategy; acidic OER

1. Introduction

Nowadays, clean energy utilization plays a significant role in human sustainability development. Green hydrogen, used as a primary energy carrier, has raised numerous attention due to its CO_2-free conversion nature.[1] Maintaining high purity of hydrogen is of vital importance for storage safety and the direct utilization in a fuel cell. PEMWEs with high purity and efficient hydrogen production are considered as the most promising approach to realize hydrogen generation for industrial application in this scenario.[2] The PEMWEs have been known since 1960 when Leonard Niedrach and Thomas Grubb firstly used ion-exchange membranes as the electrolyte in hydrogen-oxygen fuel cells.[3] PEMWEs consist of two half-cell reactions in the anode and cathode, which are known as hydrogen evolution reaction (HER) and oxygen evolution reaction (OER), respectively. HER is a two-electron transfer reaction, whereas OER is a four-electron transfer and multi-step reaction with inherent sluggish kinetics. The OER is the key half-reaction determining the overall rate and efficiency of water splitting.[4-6] Therefore, designing efficient and stable electrocatalysts to increase the rate of OER is critical for improving hydrogen evolution. In particular, the lack of effective and stable catalysts for oxygen evolution reaction has impeded its large-scale industrial application.

Preprints (www.preprints.org) | NOT PEER-REVIEWED | Posted: 25 October 2022 doi:10.20944/preprints202210.0388.v1

Iridium-based catalysts (IBCs) represent one of the most promising classes of OER catalysts due to their great intrinsic stability in acidic media. Thus, a number of innovative approaches to synthesizing IBCs have been developed in the past few years, such as molten salt method,[7, 8] pulsed laser,[9] selenic acid etching,[10] wet chemistry method,[11] solution combustion synthesis method,[12] ammonia induction method,[13] sol-gel route,[14] template method,[15] etc., which will be summarized in the third part of this review. Several excellent reviews on elucidating the mechanisms of the oxygen evolution reaction have been published, mainly focused on the adsorption evolution mechanism (AEM), lattice oxygen evolution mechanism (LOM), and the degradation mechanism of catalysts.[16-18] Meanwhile, the relationship between electronic structure, surface atomic arrangement and electrocatalytic performance has been summarized.[17] In this review, four main categories of modulation strategies for optimizing the IBCs performance for the acidic OER will be present. As shown in Fig. 1, they are doping engineering (such as alkali metal doping and transition metal doping), morphology engineering (core-shell, nanosheets, porous, etc.), crystal phase engineering (1T and 3R phase control), and support engineering (metal, metal oxide and non-metal substrates). This will give a thorough grasp of the catalysts' atomic modification tactics along with the synthesis methods, reaction kinetics, and catalytic mechanisms of IBCs.

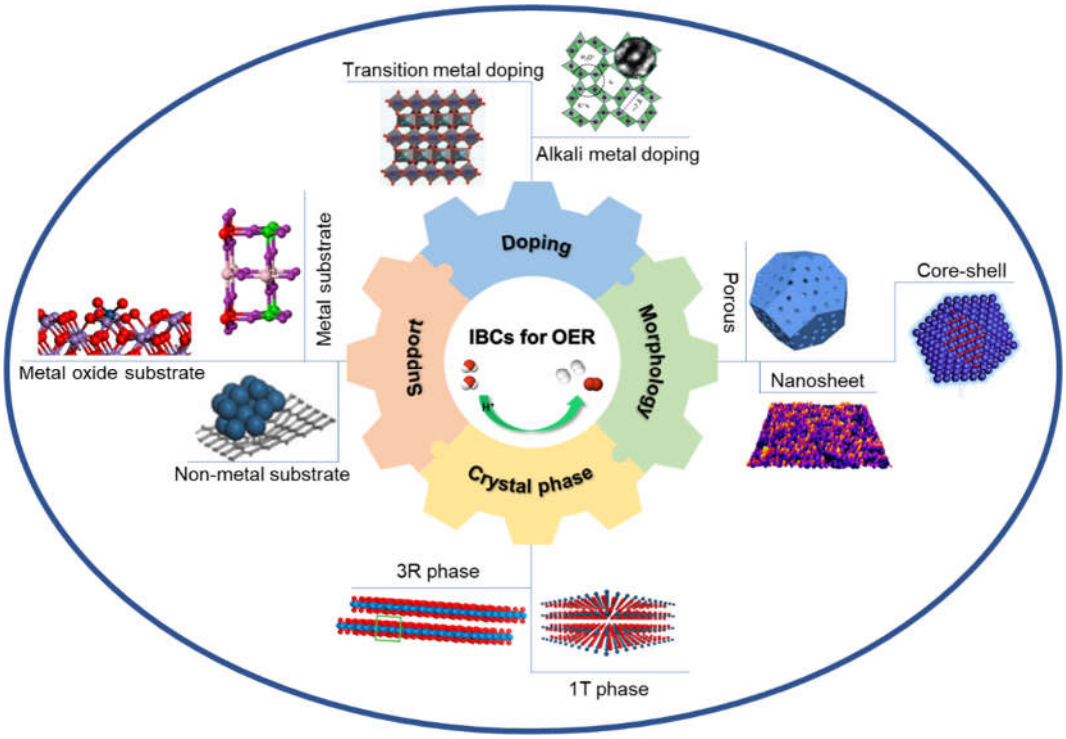

Figure 1. Schematic illustration of four general engineering strategies on IBCs. Reproduced with permission.[19] Copyright 2021, Wiley-VCH. Reproduced with permission.[20] Copyright 2017, American Chemical Society. Reproduced with permission.[21] Copyright 2018, American Chemical Society. Reproduced with permission.[22] Copyright 2019, Elsevier. Reproduced with permission.[23] Copyright 2019, Springer Nature. Reproduced with permission.[24] Copyright 2021, Sprinter Nature. Reproduced with permission.[25] Copyright 2021, Elsevier. Reproduced with permission.[26] Copyright 2020, American Chemical Society. Reproduced with permission.[27] Copyright 2021, Elsevier. Reproduced with permission.[28] Copyright 2019, Elsevier.

2. Mechanisms of Acidic OER

2.1. Conventional Adsorbate Evolution Mechanism

As shown in Fig. 2, the OER process in acid solutions can be described as[29-32]

$$* + H_2O \rightarrow *OH + H^+ + e^- \quad (1)$$

$$*OH \rightarrow *O + H^+ + e^- \quad (2)$$

Preprints (www.preprints.org) | NOT PEER-REVIEWED | Posted: 25 October 2022 doi:10.20944/preprints202210.0388.v1

$$*O + H_2O \rightarrow *OOH + H^+ + e^- \quad (3)$$

$$*OOH \rightarrow O_2\,(g) + H^+ + e^- \quad (4)$$

where * denotes the intermediate species adsorbed on the active site. As for IBCs, the active site is widely demonstrated as the coordinated unsaturated iridium (Ir) ion, and the low initial valence state of Ir ions is beneficial to weaken the Ir-O binding strength, resulting in high activity.[33] This result is in accordance with the experimental works,[24, 34] for example, Shao *et al.* confirmed that the lower valence Ir site in 1T-IrO_2 is the active site, which can modulate the binding energy of hydroxyl groups.[24] However, the AEM is not suitable for explaining the pH-dependent activity surface construction and dissolution of metal catalysts during acidic OER. The minimum theoretical overpotential for the OER in AEM is calculated to be 0.37 V, which is not satisfied with many new emerging electrocatalysts.[35, 36] Therefore, LOM has been proposed for illustrating the OER. The major difference between LOM and AEM is the source of O_2, which is derived from water molecules and lattice oxygen of oxide electrocatalysts in LOM, as depicted in Fig. 2.[37]

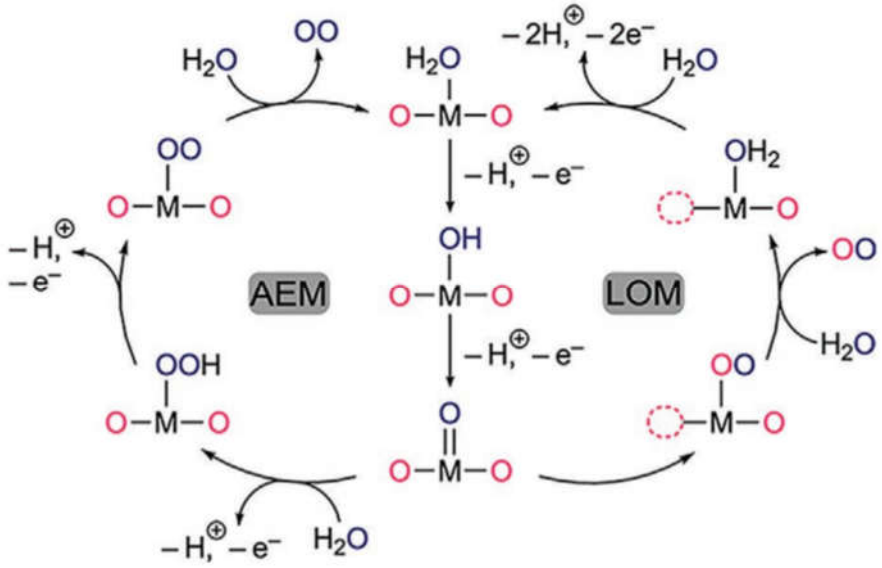

Figure 2. Proposed mechanisms for OER in acid media: adsorbate evolution mechanism (AEM) and lattice oxygen mediated mechanism (LOM). Reproduced with permission.[38] Copyright 2021, Wiley-VCH.

2.2. The Lattice Oxygen Mechanism

The acidic LOM can be concluded as follows[39, 40]

$$* + H_2O \rightarrow *OH + H^+ + e^- \quad (1)$$

$$*OH \rightarrow *O + H^+ + e^- \quad (2)$$

$$*O + O_L \rightarrow O_2 + V_o \quad (3)$$

$$V_o + H_2O \rightarrow *OH + H^+ + e^- \quad (4)$$

$$*H \rightarrow * + H^+ + e^- \quad (5)$$

where *, O_L, and V_o represent the active site, lattice oxygen, and surface oxygen vacancy, respectively. Firstly, water is adsorbed on the active sites, *OH and H^+ will be produced. Secondly, the proton is desorbed from *OH with the production of *O. Afterward, the adsorbed *O couples with the lattice oxygen to release oxygen and simultaneously forms oxygen vacancies. Finally, the V_o sites and active sites cycle the catalysis.[41] This mechanism suits for IBCs which easily forms oxygen and metal vacancies, and it has been verified experimentally and theoretically. Experimentally, IrNi@IrO_x core-shell structure, the metal vacancies induced by Ni leaching resulted in high production of O_2.[34] Theoretically, Alexandrov group used density functional theory (DFT) calculations illustrated that the metal vacancies formed through dissolution led to a high catalytic performance.[42]

Preprints (www.preprints.org) | NOT PEER-REVIEWED | Posted: 25 October 2022 doi:10.20944/preprints202210.0388.v1

3. Strategies to Enhance the Acidic OER Performance of IBCs

IBCs have been recognized as one of the best OER catalytic materials in acid media in terms of activity and stability. However, Ir is a precious metal suffering from scarcity and high cost, therefore reducing the dosage of Ir while maintaining the stability and activity of IBCs is an everlasting research topic for the acidic OER.

Up to now, many studies have focused on improving the electrocatalytic performance of IBCs and reducing the amount of Ir loading. Enhancing the intrinsic activity entails adjusting intermediate surface energy for surface adsorption and desorption as well as their electron distribution, primarily through doping engineering and support engineering. Meanwhile, crystal phase engineering and morphology engineering are effective to increase the exposure of active sites. This section will outline the theories, modulation models, and experimental progress in these four engineering modification methodologies for enhancing the activity of IBCs. The electrocatalytic performance of IBCs is summarized in Table 1.

3.1. Doping Engineering

It is worth noting that selecting the proper element composition is crucial for the OER activity and durability. In this regard, we will focus on the doping elements and their effects on the performance of IBCs in this section. Previous studies have clearly shown the importance of heteroatom doping and substitution, which can regularly alter the electronic structures of catalysts and optimize the adsorption energy of intermediates.[43-45] Transition metal and alkali metal elements listed in Fig. 3 have been utilized in doping engineering of IBCs. The OER performance of some of the these IBCs is summarized in Table 1.

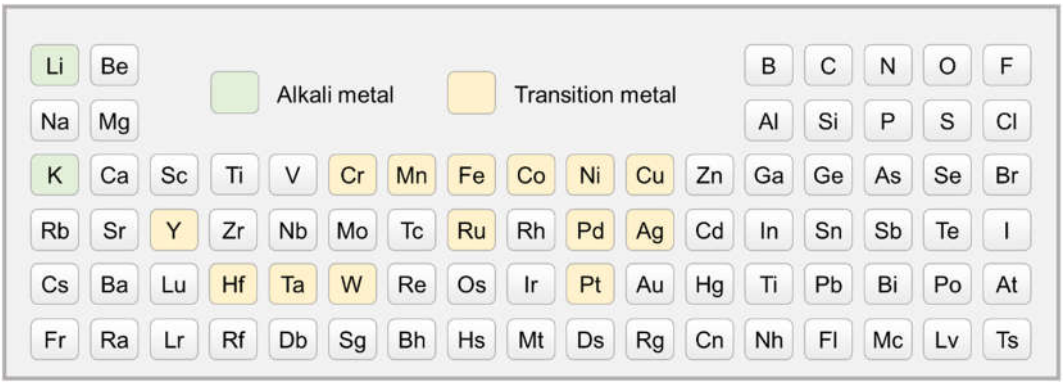

Figure 3. Screened elements that have been applied to improve the OER performance of IBCs.

Preprints (www.preprints.org) | NOT PEER-REVIEWED | Posted: 25 October 2022 doi:10.20944/preprints202210.0388.v1

Table 1. Summary of the acidic OER performance of the reported electrocatalysts.

Catalyst	Electrolyte	Activity mV@10mA cm^{-2}	Tafel Slope mV dec^{-1}	Stability	Refs
$Ru_1Ir_1O_x$	0.5 M H_2SO_4	204	71.3	110 h @100 mA cm^{-2}	19
IrRu	0.5 M H_2SO_4	300	48	/	26
RuIr-NC	0.05 M H_2SO_4	165	32	40 h @10 mA cm^{-2}	46
IrRu@Te	0.5 M H_2SO_4	220	75	20 h @100 mA cm^{-2}	26
$Ta_{0.1}Tm_{0.1}Ir_{0.8}O_{2-\delta}$	0.5 M H_2SO_4	198	64	500 h @1.5 A cm^{-2}	47
IrNi	0.1 M $HClO_4$	350	/	2 h @10 mA cm^{-2}	48
$IrCo_{0.65}$	0.1 M $HClO_4$	281	59.3	5 h @10 mA cm^{-2}	49
IrCoNi	0.1 M $HClO_4$	303	53.8	3 h @5 mA cm^{-2}	50
Ir_3Cu	0.1 M $HClO_4$	298	47.4	12 h @5 mA cm^{-2}	51
$IrHf_xO_y$	0.1 M $HClO_4$	300	60	6 h @5 mA cm^{-2}	52
$Ir_{0.1}Ta_{0.9}O_{2.45}$	0.1 M $HClO_4$	320	/	/	53
IrNi NPNW	0.1 M $HClO_4$	283	56.7	3 h @10 mA cm^{-2}	54
P-$IrCu_{1.4}$ NCs	0.05 M H_2SO_4	311	53.9	10 h @10 mA cm^{-2}	21
Li-IrO_x	0.5 M H_2SO_4	270	39	10 h @10 mA cm^{-2}	55
$IrNi_2$-PE (H^+)	0.05 M H_2SO_4	315	/	/	56
$IrNiO_x$ core-shell	0.05 M H_2SO_4	300	/	/	34
Ru@IrO_x core-shell	0.05 M H_2SO_4	282	69.1	24 h @1.55V vs RHE	22
Amorphous Ir NSs	0.1 M $HClO_4$	255	40	8 h @10 mA cm^{-2}	57
IrO_2 nanoneedles	1 M H_2SO_4	313	57	2 h @10 mA cm^{-2}	8
1T-IrO_2	0.1 M $HClO_4$	197	49	45 h @50 mA cm^{-2}	24
3R-IrO_2	0.1 M $HClO_4$	188	/	511 h @10 mA cm^{-2}	25
Ir@N-G-750	0.5 M H_2SO_4	303	50	20 h @20 mA cm^{-2}	28
Ir-$NiCo_2O_4$ NSs	0.5 M H_2SO_4	240	60	70 h @10 mA cm^{-2}	58
Ir-MnO_2	0.5 M H_2SO_4	218	59.61	650 h @10 mA cm^{-2}	27

3.1.1. Transition Metal Doping

The intercalation of transition metals has been proved to be an effective way to enhance the electrocatalytic activity of the catalysts, because it can 1) modify the *d*-band center,[59] 2) increase the concentration of highly active surface hydroxyl groups,[60] and 3) optimize interatomic distances and coordination numbers.[61] These effects, which are brought by the ligand and strain effects of foreign metals, resulted in regulated chemisorption

 doi:10.20944/preprints202210.0388.v1

behavior of intermediate species.[62, 63] Straightforward transition metal intercalation is an efficient way to overcome the limited availability and unsatisfied property of iridium, by now, the most effective transition metal is ruthenium (Ru).[26] Trace amount of Ru intercalation can enhance the activity and maintain the stability of Ir and IrO_2, due to the same valence state and similar ion radius. Apart from Ru doping, other transition metals, such as Fe,[64] Co[64, 65], Ni,[66, 67] Cu,[51, 68, 69] Hf,[70] Ta,[71] W,[72, 73] Pd,[74, 75] and Rh[76] (depicted in Fig. 3) have been applied to tailor the electronic structures of Ir and IrO_2 electrocatalysts. As shown in Fig. 4a, Sun group incorporated Ru into IrO_x through a solution combustion synthesis method. The intercalation of Ru upshifts the *d*-band center toward the Fermi level, increases the portion of the unoccupied antibonding states above the Fermi level, which promotes the binding affinity of Ir sites with oxygen intermediates (Fig. 4b). Ru dopant effectively tunes the charge redistribution, and it is confirmed by the charge density difference between $Ru_1Ir_1O_x$ and IrO_x (Fig. 4c). Ir sites with lower than +4 valence state could enhance the acidic OER performance.[19] Through reducing metal salts by refluxing ethylene glycol (EG) and using poly-vinylpyrrolidone (PVP) as a stabilizer, Qiao *et al.* were able to dope Co and Ru into Ir and synthesized a bifunctional nanocrystal for water splitting in the acidic environment.[77] They also established a linear activity dependence on reaction intermediate binding strength and trends in electrocatalytic activity with respect to reactive oxygen species concentration for OER. It is confirmed that Co leaching increases the concentration of O^{I-} species and does not alter the intrinsic shape of RuIr nanocrystals (Fig. 4d), boosted the catalytic activity in OER.[78-81] Kitagawa group reported a Ru-Ir nanosized-coral (RuIr-NC) with only 6 at.% Ir by a hot-injection process, requiring only 165 mV to achieve 10 mA cm^{-2}_{geo} (Fig. 4e). The stability was determined by the chronopotentiometry measurement under a constant current density of 1 mA cm^{-2}_{geo}, RuIr-NC shows no noticeable degradation throughout 120 h (Fig. 4f). The optimal performance of RuIr-NC results from the preferential exposed (0001) facets, as shown the in atomic-resolution aberration corrected high-angle annular dark-field scanning transmission electron microscope-scanning transmission electron microscope (HAADF-STEM) image from the selected area (Fig. 4g), the hexagonal atomic configuration shown in the nanosheets corresponds to the (0001) hexagonal closed-packed (hcp) lattice plane.[46] The (0001) facet has the lowest surface energy of hcp structures,[82] therefore, it could better protect Ru than other facets from corrosion via resisting oxidation. Through a quick pyrolysis, Jin group fabricated an IrO_2 electrocatalyst doped with tantalum and thulium with several grain boundaries, resulting in a low potential of 198 mV at 10 mA cm^{-2}. Theoretical simulations show that the torsion-strained Ir-O bonds produced by the grain boundaries synergistic effects and the doping of Ta and Ru modified the adsorption energy of oxygen intermediates, thus improved the OER activity of the IBCs.[47]

Preprints (www.preprints.org) | NOT PEER-REVIEWED | Posted: 25 October 2022 doi:10.20944/preprints202210.0388.v1

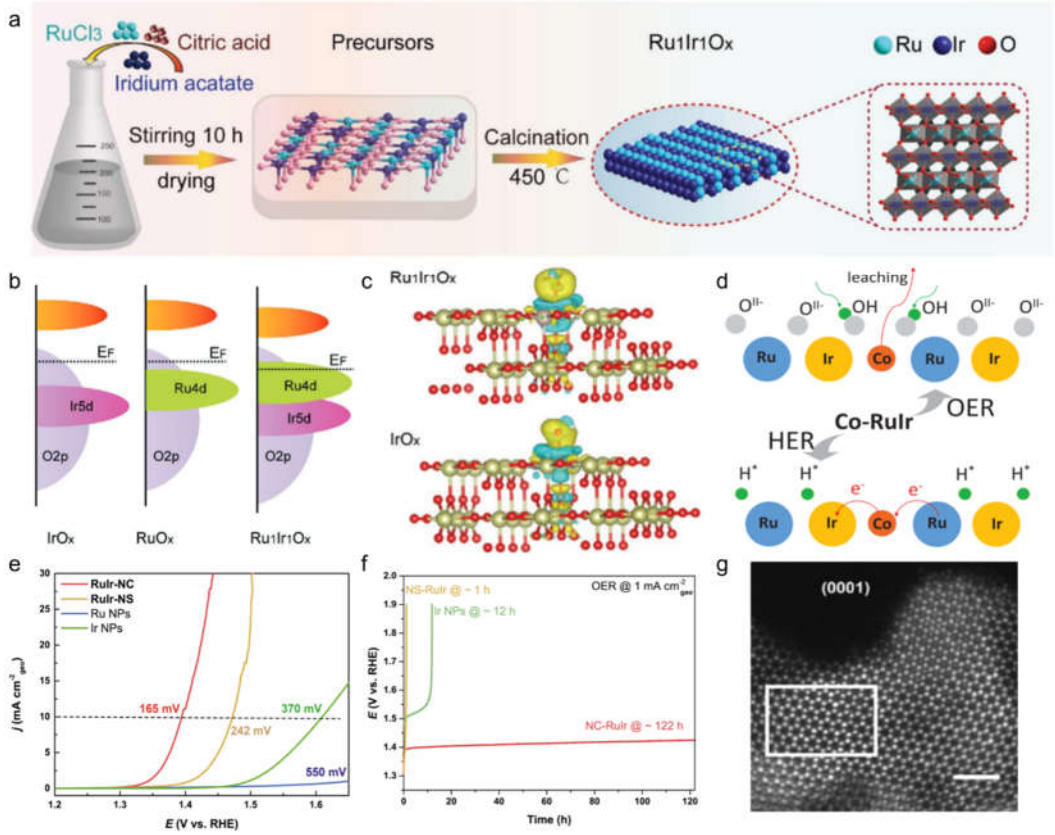

Figure 4. (a) Schematic illustration of the synthesis procedures for the prepared catalysts. (b) Schematic diagram of the band structures for IrO_x, RuO_x, and $Ru_1Ir_1O_x$. (c) Charge density difference for IrO_x and $Ru_1Ir_1O_x$ (Blue and yellow colours represent charge depletion and accumulation, respectively). Reproduced with permission.[19] Copyright 2021, Wiley-VCH. (d) Schematic of OER and HER mechanism on Co-RuIr electrocatalyst in acidic media. Reproduced with permission.[77] Copyright 2019, Wiley-VCH. (e) Geometric activity (current density normalized by electrode surface area) of RuIr catalysts (LSV profiles are obtained by cathodic scan). (f) Chronopotentiometric curves under the OER current density of 1 mA cm^{-2}_{geo}. (g) HAADF-STEM image from the selected area showing the extended (0001) plane. Reproduced with permission.[46] Copyright 2021, Springer Nature.

In order to alloy Fe, Co, and Ni with Ir, Zhang and colleagues exploited a new eutectic-directed self-templating synthesis technique. Among these alloys, IrNi shows the best OER activity with an overpotential of 283 mV to drive 10 mA cm^{-2}. Through DFT calculations, they found that these catalysts exhibit a transition-metal-dependent trend in their catalytic activity, with the regular weakening of the adsorption energy of intermediates caused by the negative shift of the *d*-band center of Ir after doping.[83] Huang *et al.* developed a surfactant-free, wet-chemical large-scale approach to synthesize IrM (M = Ni, Co, Fe) nanoparticles, achieved 10 mA cm^{-2} at a potential of only 1.58 V in 0.5 M H_2SO_4, which inducts a new direction toward modifying "acidic stable" catalysts for efficient overall water splitting.[64] Luo and co-workers reported a colloidal method for synthesizing petal-like nanodendrites IrCo alloy. The resulting $IrCo_{0.65}$ nanodendrites exhibit remarkable OER performance with an overpotential of 281 mV to achieve 10 mA cm^{-2} in 0.1 M $HClO_4$, benefitted from the unique hierarchical architecture and strong electronic interaction resulted from the synergistic alloying effect of IrCo at the atomic level.[65] Pivovar *et al.* proposed a galvanic displacement method to synthesize IrCo nanowires, their stability was enhanced through acid leaching.[84] Huang group inserted Cu into Ir crystals through a colloidal-chemical approach.[21] The effective synthesis of Ir_xCu bimetallic aerogels using nanovoids as building blocks was demonstrated by Lin's team. The specific thermochemical characteristics of Ir and Cu were revealed by the void formation mechanism using a galvanic displacement reaction and gelation process.[51] Steven fabricated $Ir_{0.89}Cu_{0.11}$ hydrous oxide nanoparticles through simply stirring solutions of $IrCl_3$ hydrate and $CuCl_2$

 doi:10.20944/preprints202210.0388.v1

hydrate in KOH under atmospheric environment.[69] Li group used a simple one-pot strategy to produce uniform Ir-Cu nanoframes with highly open structures. The key to obtaining alloy nanoframes was the dedicated control of the reduction and galvanic replacement reactions between different metals.[68]

The electronic structures of Ir can be significantly tuned by alloying with transition metals such as Fe, Co, Ni, and Cu, caused by the different ionic radii and valence states of the host and guest ions. This can optimize adsorption and desorption of adsorbates on the catalyst surface and consequently improve the OER performance.

Strasser and co-workers adjusted the ratios of Ni into IrO_2, and obtained a volcano-type OER activity curve, achieving a champion overpotential at 67% Ni with an unprecedented 20-fold improvement over IrO_2.[78] They provided atomic-scale insights into the relationship between the structure, activity, and stability of this novel type of catalyst. They suggested the coverage of reactive surface hydroxyls model to be used as a descriptor for the OER activity, indicating that the Ni dissolution and disruption of Ir-O-M motifs reduced the binding strength of the surface hydroxyls and promoted the catalytic activity.

3.1.2. Alkali Metal Doping

It is proved that alkali metal incorporation could prompt the formation of highly disordered structures of electrocatalysts, which permits the stabilization of active sites within the lattice, resulting in high activity and stability for the OER.[20, 85] Highly distorted structures are immune to suffer structural variations without being destroyed when subjected to voltage changes.[86]

Willinger and co-workers synthesized a $K_{0.25}IrO_2$-hollandite motif through a microwave-assisted hydrothermal synthesis method and compared the atomic arrangement with the commercial rutile-type IrO_2. They found that the activity of OER is correlated to the interconnected hollandite-like structural domains with short-range ordering. The rutile, hollandite, and romanechite structures viewed along the (001) direction are viewed by HAADF (Fig. 5a).[20] The tunnel-like motifs in the disordered hydroxides are possible to facilitate the transport and exchange of relevant species and play a vital role in promoting the catalytic activity. The mixed Ir oxidation state in the open three-dimensional network suggests a redox mechanism in which the change from corner- to edge-sharing, and vice versa, provides a path for release and uptake of oxygen atoms. This experimental result was further confirmed by Soon group, upon K-intercalation, a down-shift to lower energies in the averaged projected crystal orbital Hamilton population (-pCOHP) plot is observed, as shown in Fig. 5b, corresponding to a reduction in bond strength for the Ir-O bonds, implying that the intercalation of K^+ ions in the hollandite-type IrO_2 could enhance the OER performance.[87]

Preprints (www.preprints.org) | NOT PEER-REVIEWED | Posted: 25 October 2022 doi:10.20944/preprints202210.0388.v1

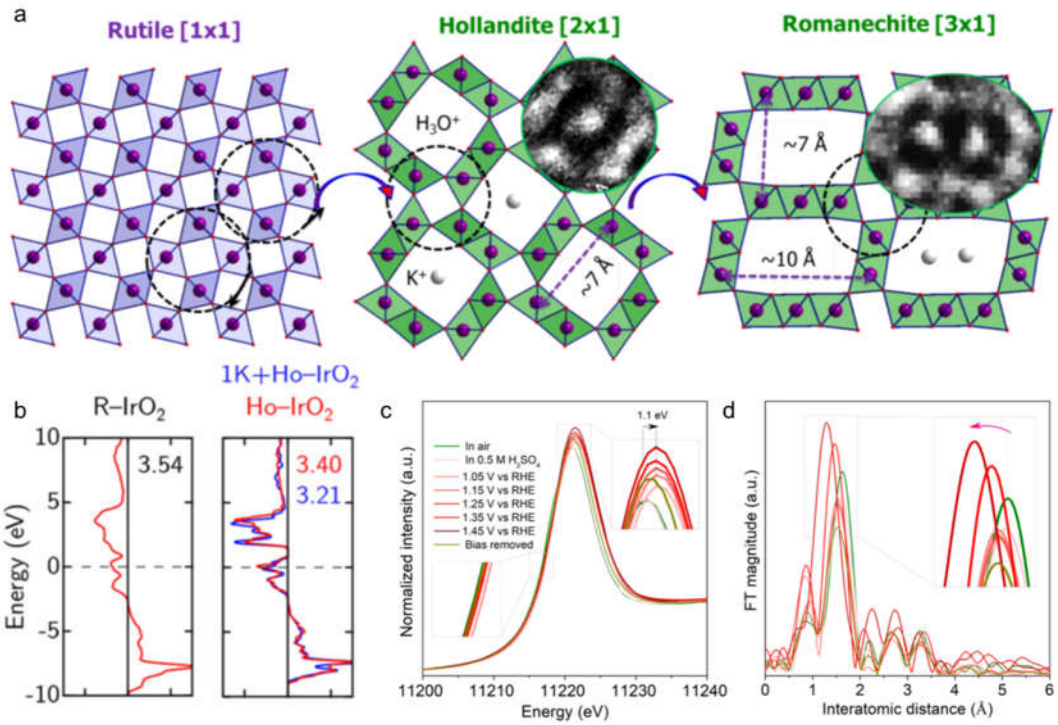

Figure 5. (a) Comparison of tunnel-like structural types with iridium clusters revealed by HAADF. Reproduced with permission.[20] Copyright 2017, American Chemical Society. (b) Averaged projected crystal orbital Hamilton population (-pCOHP) between the Ir and O atoms in R-IrO_2 and Ho-IrO_2. Reproduced with permission.[87] Copyright 2022, Springer Nature. Operando X-ray absorption spectroscopy. (c) *In-situ* XANES spectra of Li-IrO_x, (d) *In-situ* EXAFS spectra of Li-IrO_x. Reproduced with permission.[85] Copyright 2019, American Chemical Society.

Liu *et al.* synthesized an amorphous Li-IrO_x with an outstanding acidic OER overpotential of 270 mV at 10 mA cm^{-2} for 10 h of continuous operation. They pointed out that the high distortion of [IrO_6] octahedron units is the origin of the high activity.[85] Oxidation of iridium to higher oxidation states along with shrinkage in the Ir-O bond during the acidic OER catalysis process was observed by the *in-situ* X-ray absorption spectroscopy on the amorphous Li-IrO_x. As shown in Fig. 5c, X-ray absorption near edge structure (XANES) spectrum shows that the absorption peak of the Ir L^{III} edge upshifts to higher energies (from 11221.0 to 11221.5 eV) when the applied potential is increased from 1.05 to 1.45 V vs. RHE, revealing that an increase of the oxidation state of Ir in Li-IrO_x. The Ir-O bond length shrinks from 1.61 to 1.30 Å when the potential is increased from 1.05 to 1.45 V vs. RHE and recovers to its initial length after removing the external bias, as depicted in the extended X-ray absorption fine structure (EXAFS) spectrum (Fig. 5d). Much more "flexible" disordered [IrO_6] octahedrons in the amorphous Li-IrO_x as compared to the periodically interconnected "rigid" [IrO_6] octahedrons in crystalline IrO_2 can act as more electrophilic centers and thus could effectively promote the fast turnover of water oxidation.

3.2. Morphology Engineering

Morphology engineering is an efficient approach to increase the exposure of active sites. The morphology of the electrocatalysts is significantly influenced by the synthesis methods and conditions. Therefore, electrocatalysts with different morphologies synthesized by various preparation strategies will be discussed in this part, such as porous nanocrystals with chemical etching strategy, core-shell structures with a sequential polyol method, nanosheets with wet chemistry, and metal melting methods.

3.2.1. Porous Structure

Preprints (www.preprints.org) | NOT PEER-REVIEWED | Posted: 25 October 2022 doi:10.20944/preprints202210.0388.v1

Porous structure is beneficial for enhancing the catalytic performance of IBCs in acidic OER, due to its extremely large surface areas, accessible pores and selective adsorption.[88, 89] Huang group developed a facile chemical dealloying strategy to fabricate porous $IrCu_x$ and $IrNi_x$ nanocrystals, which provides a promising method for preparing three-dimensional porous IBCs.[21, 56] They used nitric acid to selectively leach Cu from the pristine solid $IrCu_x$ alloy nanocrystals (Fig. 6a) and compared the activity and stability with the pristine and porous nanocrystals.[21] Many pores (<5 nm) can be observed within the particles, resulting in the interrupted lattice fringe in the particle (Fig. 6b). Similar porous structures could provide abundant defects that are beneficial to the electrocatalytic performance.[90, 91] The optimized porous $IrCu_{1.4}$ NCs show excellent OER activity with only 311 mV of overpotential to reach 10 mA cm^{-2} in 0.05 M H_2SO_4.

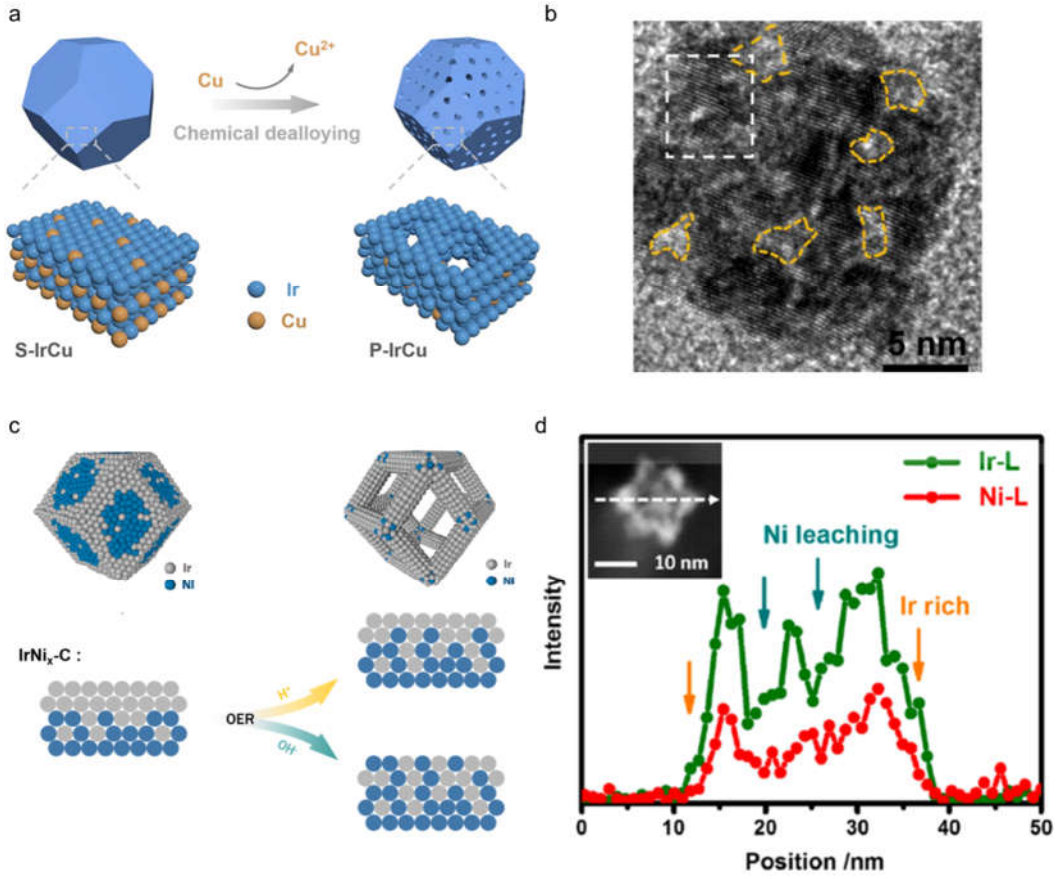

Figure 6. (a) Schematic illustration of the transformation from S-IrCu to P-IrCu NCs via chemical dealloying. Reproduced with permission.[21] Copyright 2018, American Chemical Society. (b) HRTEM image of P-$IrCu_{1.4}$. The yellow dashed curve highlights the pores in the particle. Reproduced with permission.[21] Copyright 2018, American Chemical Society. (c) Schematic representation of the surface structure changes of $IrNi_x$-C after OER electrocatalysis under acidic conditions. Reproduced with permission.[56] Copyright 2018, American Chemical Society. (d) Line scan analysis of the $IrNi_2$-C. Reproduced with permission.[56] Copyright 2018, American Chemical Society.

Simultaneously, the dissolution of Ni component in the acidic electrolyte creates an Ir-skin structure with Ni in the subsurface, which is comparable to the effect of chemical etching and results in the OER performance improvement (Fig. 6c). The line scans (Fig. 6d) further proved that the inner Ni was leached, leading to the Ir-rich frame during OER catalysis, exhibiting a similar behavior as the chemical etching processes.[56]

3.2.2. Core-Shell Structure

Core-shell structures have advantages in enhancing the catalytic performance of electrocatalysts due to 1) the charge redistribution at the metal core-shell heterojunction's

Preprints (www.preprints.org) | NOT PEER-REVIEWED | Posted: 25 October 2022 doi:10.20944/preprints202210.0388.v1

favorable surface valence states; and 2) the core-shell nanostructure's protection of inner sites, which could reduce metal cation dissolution rates.[92, 93]

IrNi@IrO_2 core-shell structure was obtained by Strasser *et al*. through controlling the surface oxidation of Ir and dealloying selective surface Ni, triples the activity of the OER over IrO_2 catalyst. Furthermore, they demonstrated that Ni leaching occurs during the hole-doped $IrNiO_x$ core-shell catalysis, resulting in lattice vacancies, which shortens Ir-O metal ligand bonds and increases the number of *d*-band holes in the iridium oxide shell.[34] The metal vacancies induced by the metal leaching could attribute to a high degree of Ir-O covalence state and enhance the IBCs catalytic performance. Qiao and colleagues enhanced the activity and stability of IrO_2 catalysts by inducing charge redistribution inside the heterostructure electrocatalysts. Through a sequential polyol method under refluxing conditions, they synthesized Ru@IrO_x core-shell structures with the synergistic interaction in terms of electron and structure (Fig. 7a).[22] The increased valence of the iridium shell (Fig. 7b) and the decreased valence of the ruthenium core greatly boosted the OER activity and stability in an acid medium (Fig. 7c). The universal methods to create oxygen vacancies in metal complexes include sodium borohydride and hydrogen reduction, plasma irradiation, and thermal annealing under argon or air conditions.[90, 94] Chen group added an excess amount of sodium borohydride to co-reduce the Ir and metal, creating oxygen vacancies and achieving an excellent OER activity, as well as reduced the iridium loading through synthesizing Ir/Fe_4N core-shell particles with nitride cores.[93] The DFT calculated ΔE [ΔG(*O) - ΔG(*OH)] values on IrO_2/Fe_4N are higher than those of on the IrO_2(110) and IrO_2/Ni_4N (Fig. 7d), which means that Ir/Fe_4N core-shell structure could prompt the OER activity close to the predicted volcano peak. The EXAFS spectrum measured at an open-circuit voltage (OCV) shows that the Ir is coordinated with Ir and Fe, and Fe is in the iron-nitride state as the core, which maintained stable during the acidic electrocatalysis (Fig. 7e, f).

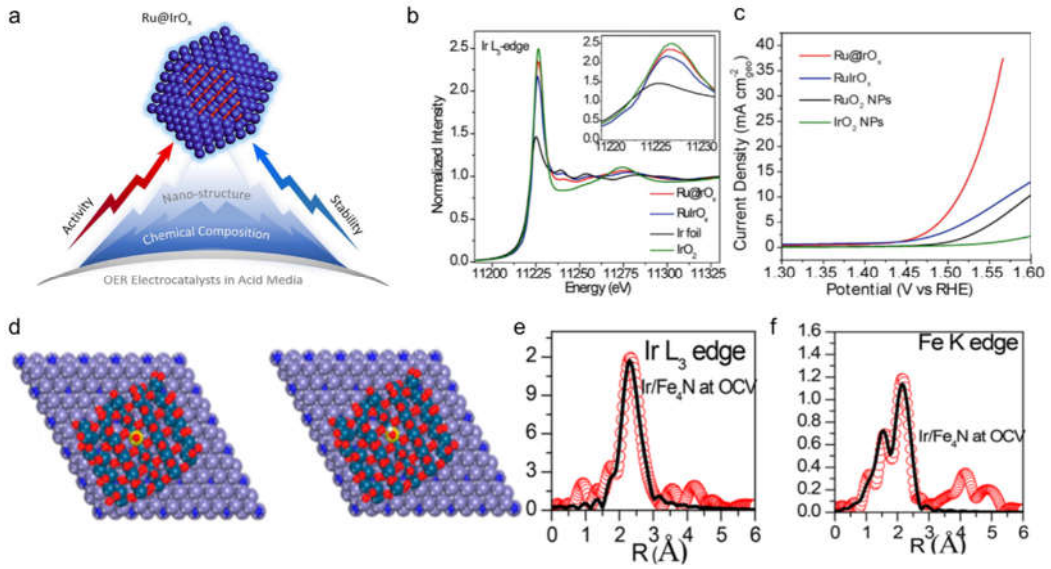

Figure 7. (a) Scheme of the Ru@IrO_x core-shell structure nanocrystal. (b) Ir L_3-edge synchrotron-based XANES data of Ru@IrO_x and RuIrO_x electrocatalysts and the references. (c) LSV curves normalized by using geometrical surface area of various electrocatalysts in N_2-saturated 0.05 M H_2SO_4 solutions. Reproduced with permission.[22] Copyright 2019, Elsevier. (d) DFT-optimized geometries of IrO_2(110), O adsorbed on IrO_2(110), OH adsorbed on IrO_2(110), IrO_2/Fe_4N, O adsorbed on IrO_2/Fe_4N, and OH adsorbed on IrO_2/Fe_4N, respectively. Ir, dark blue; Fe, purple; O, red; N, light blue; H, white. Yellow metal site represents an oxygen vacancy site for the adsorption of OER intermediates O and OH. (e) Ir L_3 EXAFS spectrum for Ir/Fe_4N at OCV. (f) Fe K EXAFS spectrum for Ir/Fe_4N at OCV. Reproduced with permission.[93] Copyright 2018, American Chemical Society.

Preprints (www.preprints.org) | NOT PEER-REVIEWED | Posted: 25 October 2022 doi:10.20944/preprints202210.0388.v1

3.2.3. Nanosheet

Two-dimensional (2D) nanomaterials have gradually attracted extensive research attentions since Geim and Novoselo obtained graphene *via* the exfoliation method in 2004.[95] 2D materials have been widely used in the field of electronics, biology, energy, and catalysis due to their distinctive physical, chemical, optical, and electrical properties. In particular, nanosheets represent a new class of electrocatalysts with enhanced acidic OER performance, which is attributed to three reasons: 1) More atoms are exposed as active sites;[96, 97] 2) The sheet-like structures can offer large surface area to contact with the electrolyte and thus boost the reaction between reactants and catalysts;[96-98] 3) The robust and flexible nanosheet structure may be more stable than some other nanomaterials.[99] Wet-chemical reduction synthesis method is regarded as the most efficient way to prepare nanosheets with high catalytic performance.[100] A good example is the formation of mesopores in the plane of 2D Ir nanosheets by Yamauchi and colleagues through a wet chemical reduction process (Fig. 8a). The mesoporous Ir nanosheets demonstrated exceptional high activity with an overpotential of 240 mV at 10 mA cm^{-2} in 0.5 M H_2SO_4, due to abundant highly accessible exposed surface active sites.[101]

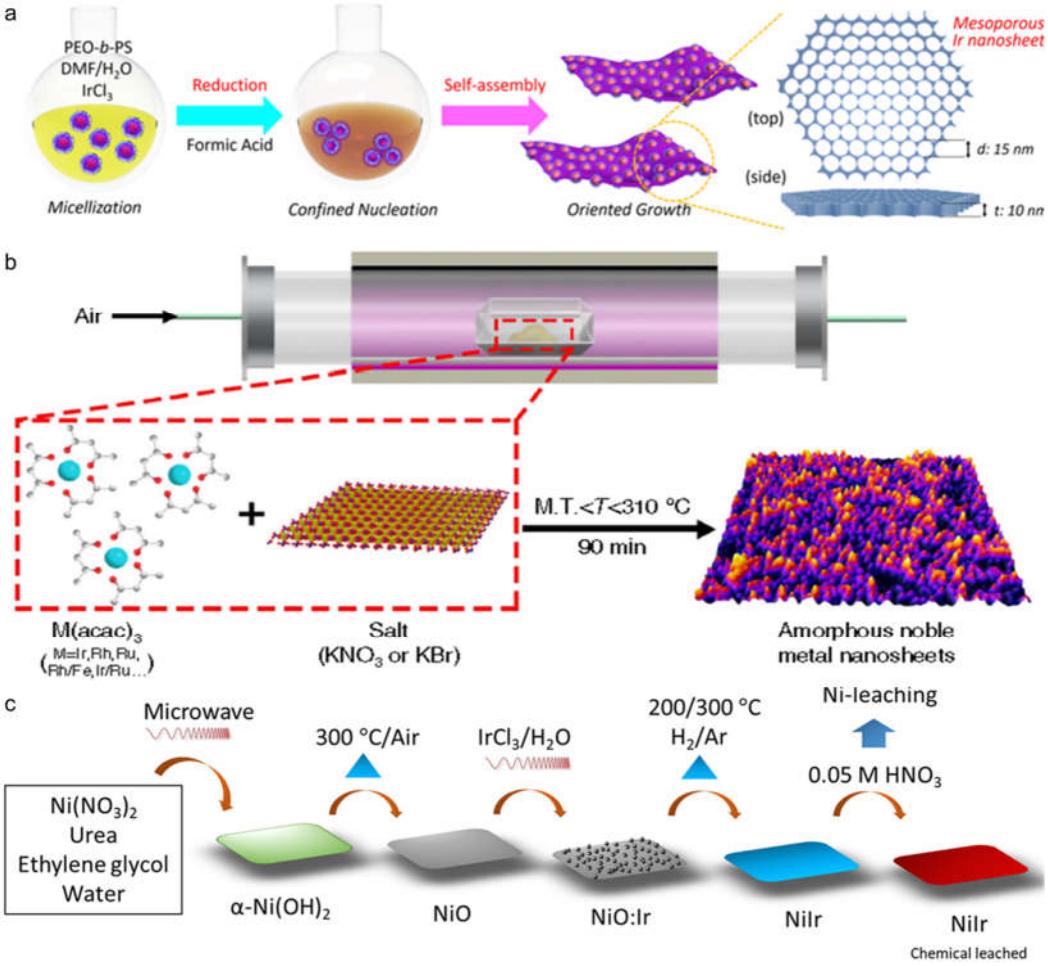

Figure 8. Schematics of strategies for synthesizing nanosheets. (a) Wet chemistry synthesis method. Reproduced with permission.[101] Copyright 2018, American Chemical Society. (b) Solid melting method. Reproduced with permission.[23] Copyright 2019, Springer Nature. (c) Microwave-assisted method. Reproduced with permission.[67] Copyright 2018, American Chemical Society.

Amorphous electrocatalysts are favorable for achieving high catalytic activity and long-term stability because of their rapid electron and mass transfer channels, structural flexibility, and resistance to aggregation.[23, 102] Li and co-workers developed a comprehensive approach for fabricating amorphous noble metal nanosheets with customizable atom

Preprints (www.preprints.org) | NOT PEER-REVIEWED | Posted: 25 October 2022 doi:10.20944/preprints202210.0388.v1

arrangement *via* the direct annealing a mixture of metal acetylacetonate and alkali salts (Fig. 8b).[23] The amorphous Ir nanosheets show excellent activity and durability, which is benefitted from the abundant active sites and unique atomic structures. It is important to note that the synthetic temperature should lie between the melting points of metal acetylacetonate and alkali salt because annealing below the melting point of metal acetylacetonate will not drive the reaction, whereas annealing above the melting point of alkali salt will produce crystalline materials. This molten salt synthesis method can be used for industrial applications due to its simple preparation procedure and scalability.[103, 104] Rhodes *et al.* coupled the microwave assisted hydrothermal procedure with the thermal reduction treatment to optimize the electrocatalytic performance of NiIr nanosheet (Fig. 8c).[67] They found that the thermal reduction temperature strongly affects the IBCs surface structure and OER activity. In addition, other IBCs, such as bimetallic nanowires,[84] ultrathin IrO_2 nanoneedles,[8] trimetallic nanocages[105] have been reported to perform excellently in terms of activity and durability in acidic OER.

3.3. Crystal Phase Engineering

Crystal phase engineering refers to changing the arrangement of atoms to regulate the physical and chemical properties of materials, which can optimize the performance of various electrocatalysts because of its ability to govern electronic structure and coordination chemistry.[106, 107] Unconventional crystal phases may lead to superior electrocatalytic performance of IBCs. For example, using a home-made mechano-thermal reactor (Fig. 9a) with a heating rate of 10 °C min^{-1} and a rotation speed of 6 rpm, Shao group synthesized the tetragonal phase IrO_2 (1T-IrO_2) with an ultralow overpotential of 197 mV to reach the current density of 10 mA cm_{geo}^{-2}.[24] As shown in the X-ray diffraction (XRD) pattern (Fig. 9b), the peaks show the layered structures along the c-axis are corresponding to the (0001) and (0002) diffraction planes, respectively. The peak at about 12.81° is an important fingerprint to distinguish the unit-cell parameter c along c direction, which is calculated to be ~6.91 Å. The key to the high-performance acidic OER is the optimized Ir active site in the 1T-phase and the ultrathin 2D structure. Computational calculations reveal that the catalytic origin of 1T-IrO_2 in OER can be attributed to the optimized free energy that increases the binding hydroxyl groups on Ir atoms (Fig. 9c). Simultaneously, the same group obtained the rhombohedral phase IrO_2 (3R-IrO_2) through a microwave-assisted mechano-thermal method (Fig. 9d). The trigonal crystal structure of 3R-IrO_2 was revealed by the XRD pattern, as depicted in Fig. 9e. Since it only completely transforms into rutile-IrO_2 at an annealing temperature of up to 900 °C, 3R-IrO_2 is a stable phase, resulting in an excellent stability under the current density of 10 mA cm_{geo}^{-2} (the overpotential of 3R-IrO_2 shifts only about 30 mV after 511 h). Both the interlayer and intralayer space, when combined with the intralayer Ir vacancies, are beneficial for the fast proton diffusion (Fig. 9f). A completely new working pathway for the acidic OER is provided by the improved proton transportation through the in-plane 2D confining structure and the vertical direction through iridium vacancies.[25]

Preprints (www.preprints.org) | NOT PEER-REVIEWED | Posted: 25 October 2022 doi:10.20944/preprints202210.0388.v1

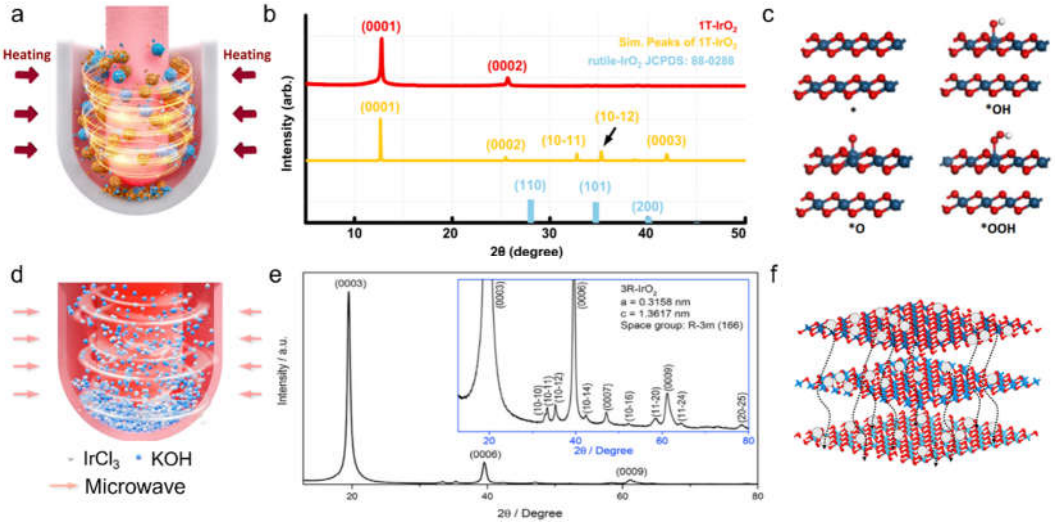

Figure 9. (a) Schematic representation of the mechano-thermal reactor for preparing 1T-IrO_2, where the mechanical and thermal operations are controlled simultaneously. The blue and yellow balls indicate $IrCl_3$ and KOH, respectively. (b) XRD pattern of 1T-IrO_2. (c) The free energy profile of OER over the 1T-IrO_2. Reproduced with permission.[24] Copyright 2021, Sprinter Nature. (d) The schematic synthesis of the microwave-assisted mechano-thermal method for 3R-IrO_2. (e) XRD pattern of 3R-IrO_2. (f) The proton transportation pathway along interlayers and intralayers in 3R-IrO_2. Reproduced with permission.[25] Copyright 2021, Elsevier.

3.4. Support Engineering

Support materials are of vital importance for PEMWEs but have not been intensively studied for catalyst design until recent years. Strasser and co-workers demonstrated a support-stabilizing effect that contributes to the corrosion durability of Ir catalyst in acidic water splitting. Through adjusting the electronic interaction between catalyst and support, the growth of higher-valent Ir oxides and the subsequent dissolution can be effectively restrained.[108] Moreover, both Ir and Ru are precious rare metals in the Earth's crust, therefore using catalysts loaded on conductive supports is a favorable strategy to reduce the amount of precious metal required to satisfy the practical and large-scale applications.[109, 110] Up to now, various substrates such as carbon, Ni foam, TiO_x, and antimony-doped tin oxide (ATO) have been explored to support the electrocatalysts for water splitting.[102, 111-114] However, carbon and Ni can hardly be used in practice, as they would be oxidized at relatively low anodic potentials. Even for the ATO support materials, it may become unstable under the harsh acidic OER conditions.[115] The suitable support should be corrosion-resistant and electronically adjustable. Metal, metal oxide, and non-metal substrates have been utilized to enhance the activity and stability of acidic OER, which will be summarized in this section.

3.4.1. Metal Substrate

Due to the synergic effects, the combination of Ir and metal substrate may give rise to enhanced electrocatalytic activity and stability over the individual components. For instance, Xiong *et al.* fabricated a biphasic alloy using a water-cooling copper mold casting method under a high-purity argon atmosphere.[116] As shown in the transmission electron microscopy (TEM) image (Fig. 10a), region A (the IrW phase) and B (the W-rich phase) are interconnected in the alloy, dominantly resulted from the rapid cooling rate during melting. This support-stabilizing effect prevented the surface Ir from agglomeration, achieved an optimized performance that the current density reaches 2 A cm^{-2}_{geo}, but the overpotential still maintains a low value of ~497 mV, which demonstrates that this catalyst has great potential for application in industrial PEM devices. To gain a thorough understanding of the catalyst's dissolving behavior during the acidic OER, they combined the chronopotentiometry test at 100 mA cm^{-2}_{geo} with the inductively coupled plasma-optical emission

Preprints (www.preprints.org) | NOT PEER-REVIEWED | Posted: 25 October 2022 doi:10.20944/preprints202210.0388.v1

spectrometry (ICP-OES) characterization. The measurement indicates that trace amount of Ir was dissolved (up to 0.11 mg L^{-1}) in the 0.5 M H_2SO_4 along with the 120 h stability test, which is an order of magnitude less than the W leaching (up to 3.25 mg L^{-1}) into the electrolyte (Fig. 10b). They modelled the differential charge densities of the IrO_2 cluster adsorption on the IrW (002) surface to further study the interfacial electron-transfer process (Fig. 10c). The charge distribution of Ir and O atoms is altered with the support of the IrW. Particularly, Ir atoms lose electrons whereas O atoms gain electrons. The accumulation of positive charges at Ir atoms could promote the formation of the catalytical active IrO intermediates,[117] thereby boosting the OER performance. These findings show an electrocatalytic activity and stability win-win strategy, which is attributed to the catalyst-support interactions.

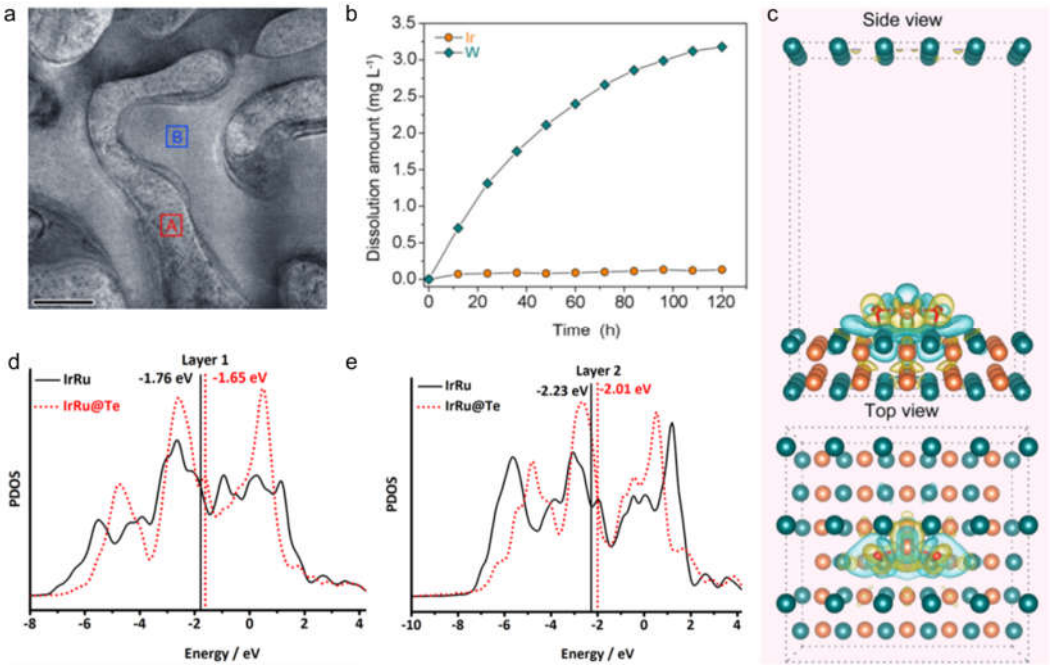

Figure 10. (a) TEM image of the W-Ir-B alloy. (b) Dissolution amount variation of Ir and W elements during the 120-h acidic OER test at 100 mA cm^{-2}_{geo}. (c) Computed differential charge density of the IrO_2 cluster adsorbed to the IrW (002) surface. Yellow and blue bubbles represent the positive and negative charges with an iso-value of 0.005 e $Å^{-3}$, respectively. Reproduced with permission.[116] Copyright 2021, Sprinter Nature. (d, e) Computed PDOS of IrRu@Te and unsupported IrRu catalysts. The vertical solid and dotted lines represent the *d*-band center of unsupported IrRu and IrRu@Te, respectively. The Fermi level is set to zero. Reproduced with permission.[26] Copyright 2020, American Chemical Society.

Liu group reported a one-pot hydrothermal method to synthesize IrRu@Te, where IrRu clusters scattered over an amorphous tellurium nanoparticle support.[26] IrRu@Te exhibits better performance compared with that of the unsupported IrRu and the commercial Ir- and Ru-based catalysts. This can be attributed to the charge transfer between IrRu and the support, which is verified by the projected density of state (PDOS) results. As shown in Fig. 10d and e, the PDOS of the catalyst shifts toward the Fermi level after loading IrRu on Te (IrRu@Te), and the corresponding *d*-band center shifts from -1.76 to -1.65 eV in Layer 1 and from -2.23 to -2.01 eV in Layer 2.

3.4.2. Metal Oxide Substrate

There has been growth of interest in the metal dispersed on metal oxide substrates prepared by deposition method.[118] The surface of these systems possesses a number of unique electronic, adsorption, and reaction properties due to their multicomponent structure, which is beneficial to optimizing the catalytic performance of IBCs. Yan and

Preprints (www.preprints.org) | NOT PEER-REVIEWED | Posted: 25 October 2022 doi:10.20944/preprints202210.0388.v1

colleagues prepared Ir single atoms on ultrathin $NiCo_2O_4$ porous nanosheets through a co-electrodeposition method (Fig. 11a). As shown in Fig. 11b, the HAADF-STEM image of Ir-$NiCo_2O_4$ NSs indicates that the Ir single-atoms (Ir-SAs) scatter on the $NiCo_2O_4$ porous nanosheet. It can be concluded from the EXAFS spectra (Fig. 11c) that the Ir-$NiCo_2O_4$ NSs sample only has the Ir-O scattering path, because the peaks of second Ir-Ir^{I} shell and the third Ir-Ir^{II} shell from Ir-$NiCo_2O_4$ NSs cannot be detected, while they are observable in the commercial IrO_2. The atomic Ir sites could enhance the electronic activity of surface lower coordinated Co sites nearby V_o, enabling improvements of the surface electronic exchange-and-transfer capabilities, thus the catalyst shows superior OER activity with an overpotential of 240 mV at 10 mA cm^{-2}, and 70 h stability in acid media (Fig. 11d).[119] Ge *et al.* firstly demonstrated lattice oxygen redox in Ir single-sites supported with MnO_2 (Fig. 11e), the EXAFS results (Fig. 11f) reveal that the covalency contraction between Ir and O accounts for about 5% Ir-O bond length shrinking in Ir-MnO_2 (1.57 Å) compared to IrO_2 (1.65 Å), allows for more than 42 times mass activity than that of the commercial IrO_2 as well as over 650 h stability (Fig. 11g).[27]

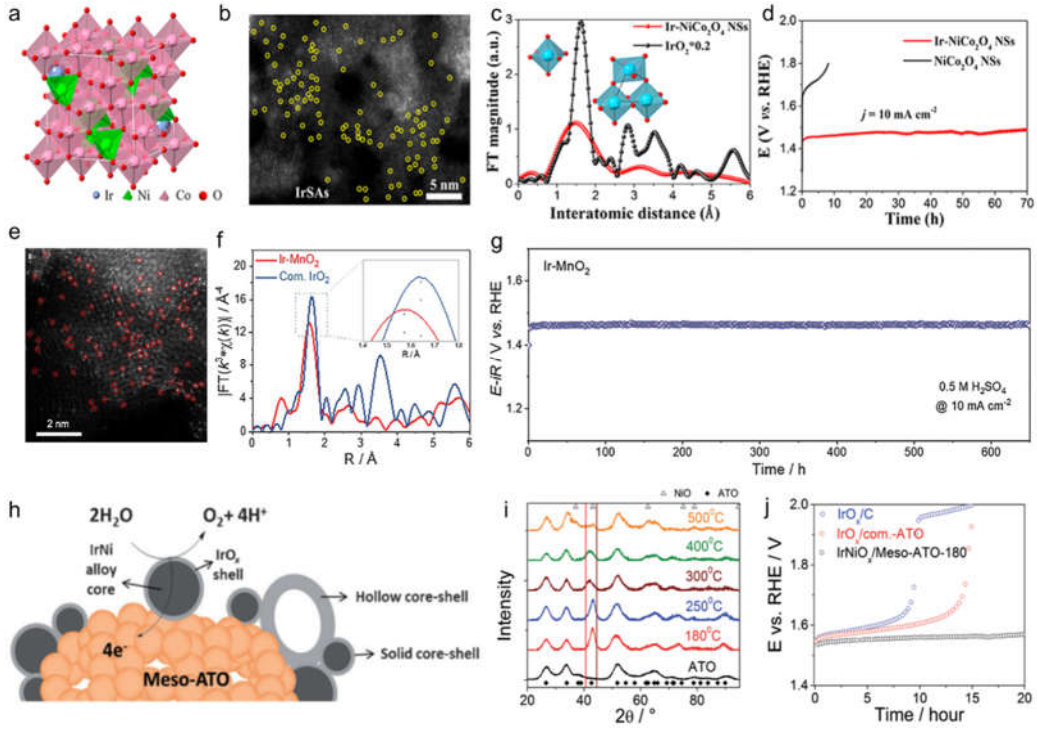

Figure 11. (a) Structure of Ir-$NiCo_2O_4$ NSs. (b) HAADF-STEM image of Ir-$NiCo_2O_4$ NSs, indicating the Ir-SAs. (c) EXAFS spectra of IrO_2 and Ir-$NiCo_2O_4$ NSs. (d) Chronoamperometric response of $NiCo_2O_4$ and Ir-$NiCo_2O_4$ NSs for OER at 10 mA cm^{-2} in 0.5 M H_2SO_4. Reproduced with permission.[119] Copyright 2020, American Chemical Society. (e) Representative high-magnification HAADF-STEM image of Ir-MnO_2, in which the bright spots highlighted by the red circles are ascribed to Ir single atoms. (f) Fourier-transforms of k_3-weight Ir L_3-edge EXAFS spectra for Ir-MnO_2 and commercial IrO_2. (g) Chronopotentiometric response of Ir-MnO_2 for OER at 10 mA cm^{-2}. Reproduced with permission.[27] Copyright 2021, Elsevier. (h) Scheme of the oxygen evolution reaction on the IrO_x shell of $IrNiO_x$ core-shell NPs supported on Meso-ATO. (i) XRD patterns, vertical solid lines indicate (111) database reflections of pure metallic Ir and Ni; open triangles and solid rhombuses indicate database main reflections of NiO and antimony-doped tin oxide, respectively. (j) Constant current chronopotentiometric stability measurements at a current density of 1 mA cm^{-2}. Reproduced with permission.[120] Copyright 2015, Wiley VCH.

Similarly, Strasser and colleagues anchored $IrNiO_x$ core-shell particles on high-surface-area mesoporous antimony-doped tin oxide ($IrNiO_x$/meso-ATO) through electrochemical Ni leaching and subsequent Ir oxidation (Fig. 11h). They probed the influence of the annealing temperature on the durability of $IrNiO_x$/meso-ATO and uncovered the

 doi:10.20944/preprints202210.0388.v1

detrimental impact of segregated NiO phases. As shown in Fig 11i, the reflection peak between 40 and 45° (corresponding to (111) plane of the alloy crystallites)[121] shifted to smaller 2θ with the annealing temperature is increased, indicating that enrichment in Ir at decreased crystalline size. They found that $IrNiO_x$/meso-ATO-180 annealed at 180 °C shows an outstanding stability under constant current load for approximately 20 h (Fig. 11j).[120] To reduce the usage amount of Ir, Daniel *et al.* employed a solvothermal reduction to achieve a remarkable low Ir bulk density (approximately 0.08 g cm^{-3}) using microporous ATO-supported iridium oxides catalysts. This electrocatalyst reaches a current density of 63 A g_{Ir}^{-1} at an overpotential of 300 mV.[122] Mendes made a comparison of activity and stability among Sb-SnO_2 (IrO_x/ATO), In-SnO_2 (IrO_x/ITO) and SnO_2 supports, demonstrating that In-SnO_2 offers the optimum balance of activity and stability while also lowers the amount of Ir.[123] Thomas group developed a one-step molten method to disperse iridium oxide nanoparticles in titania, which possesses a high surface area for contact between the electrolyte and catalyst, leading to a high OER performance.[124]

3.4.3. Non-Metal Substrate

High electrical conductivity and stability of non-metal substrate are indispensable for the catalyst supports to achieve desirable electrocatalytic performance. Therefore, defective graphene and carbon nanotubes are selected to be substrates for enhancing the electrocatalytic performance of IBCs. Typically, iridium-copper oxide nanoclusters supported on defective graphene (DG) ($IrCuO_x$@DG) were fabricated by Zhu group using a facile Ar plasma treatment. The subsequently formed porous IrO_x nanoclusters dispersed on DG (Fig. 12a) sample was obtained through acid leaching to remove Cu.[125] In 0.5 M H_2SO_4, the P-IrO_x@DG outperforms the commercial IrO_2 and O-IrO_x@DG due to the introduction of unsaturated Ir atoms by Cu removal. By doping Ir single atoms into Fe nanoparticles and then dispersing Ir-SA@Fe onto the surface of nitrogen-doped carbon nanotubes (Ir-SA@Fe@NCNT), Cai and co-workers were able to double-encapsulate Ir, as illustrated in Fig. 12b.[126] Ir-Fe coordination considerably suppresses the oxidation of Ir atoms, which lowers the adsorption strength of oxygen intermediates and achieves an overpotential of 250 mV at 10 mA cm^{-2}. Moreover, Ir-Fe bonding interaction has successfully prevented the dissolution of Ir atoms, and the encapsulation of Ir-SA@Fe nanoparticles into nitrogen-doped carbon nanotubes (Fig. 12c) further inhibited this process, assuring the robust stability (10 mA cm^{-2} for 12 h without obvious attenuation).

Through the annealing treatment, Li group dispersed ultrasmall Ir nanoparticles on nitrogen-doped graphene sheets (Ir@N-G-750), which exhibited enhanced durability with undecayed current density of 20 mA cm^{-2} for 20 h continuous electrocatalysis. DFT calculations demonstrated that affluent Ir-N (especially the pyridinic-N) coordination stabilizes the Ir clusters (Fig. 12d), leading to an obviously reduced electron affinity of Ir atoms. The weakened Ir-O bonding due to the interfacial charge transfer accounts for an improved catalytic activity with an overpotential of 303 mV at 10 mA cm^{-2}.[28]

Preprints (www.preprints.org) | NOT PEER-REVIEWED | Posted: 25 October 2022 doi:10.20944/preprints202210.0388.v1

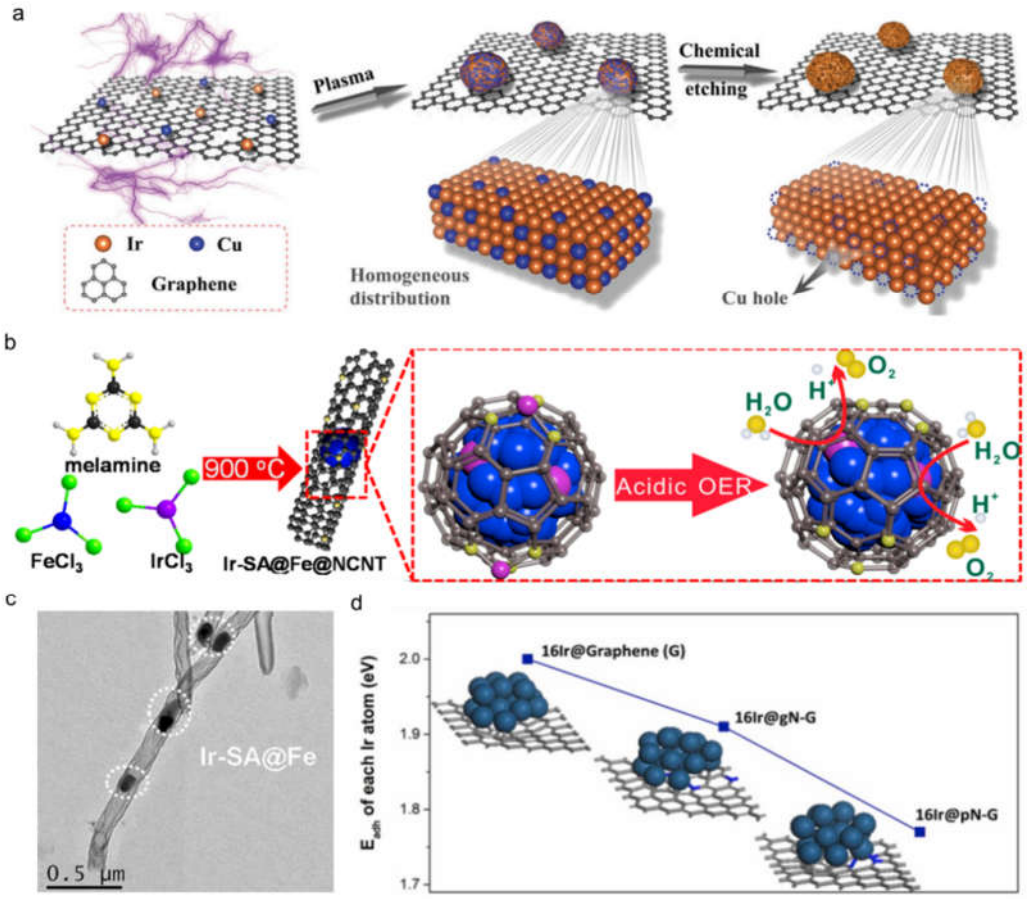

Figure 12. (a) The schematic illustration for the synthesis of P-IrO_x@DG hybrids. Reproduced with permission.[125] Copyright 2021, Wiley-VCH. (b) Schematic illustration of the preparation of Ir-SA@Fe@NCNT electrocatalyst. (c) HR-TEM of Ir-SA@Fe@NCNT electrocatalyst. Reproduced with permission.[126] Copyright 2020, American Chemical Society. (d) The variation of calculated adhesion energies of Ir in different models. Reproduced with permission.[28] Copyright 2019, Elsevier.

4. Conclusions and Perspectives

Up to now, tremendous breakthroughs have been accomplished in improving the catalytic performance of IBCs for the acidic OER. In this review, we systematically summarized four primary engineering strategies and the most recent advances of developing IBCs in acidic OER, including doping engineering, morphology engineering, crystal phase engineering, and support engineering. Besides, common synthesis methods for preparing different morphologies of IBCs are illustrated, which provide a thorough and explicit guidance for synthesizing and optimizing the catalytic performance of IBCs in acid environment. Additionally, the effect of various engineering strategies and reaction mechanisms are discussed. To overcome the limitations of IBCs, more systematic and in-depth work should be continuously conducted, both theoretically and experimentally. It is indispensable to carry out in-depth studies on the electrocatalytic and dissolution mechanisms as well as to develop new universal easy-to-use synthesis techniques, before promoting their mass-application in commercial fields. Although IBCs for acidic OER have been well developed, further work should be done on the following aspects.

(1) Deep Insight into the Reaction and Dissolution Mechanisms of IBCs in Acidic OER

Although various explanations for the reaction and dissolution of acidic OER have been proposed, it is still unknown whether a universal reaction mechanism for the IBCs exists. A feasible method for simulating the reaction and dissolution mechanisms during acidic OER of IBCs is combining DFT calculations with isotope labeling studies and the *in-situ* operando characterizations.

 doi:10.20944/preprints202210.0388.v1

On the one hand, the physicochemical properties related to oxygen binding energy have been utilized as the descriptors to predict the activity of the electrocatalysts, including *d*-band center,[127] e_g orbital occupancy,[128] *p*-band center,[129] charge transfer energy,[130] line relationship between adsorption energy of *OH and *OOH intermediates ("*" represents active sites.),[131] "generalized" coordination numbers,[116] content of surface hydroxyl groups,[67] etc. More accurate and suitable descriptors are required to reveal the reaction and dissolution mechanisms of various IBCs during OER process in acid media.

On the other hand, *in-situ* techniques have been applied to study the electronic structures and coordination conditions of electrocatalysts in the OER, for example, XANES and EXAFS analytical techniques have been used to reveal the valence state of Ir and the bond length of Ir-M or Ir-O, respectively. Isotope-labelling analytical technique has been applied to reveal the reaction mechanism of acidic OER. More advanced *in-situ* characterization techniques, such as the *in-situ* ICP with a scanning flow cell (SFC) should be applied to investigate the surface reconstruction and reaction intermediates of catalysts during the OER.

(2) Controllable and Feasible Synthesis of Low-Cost IBCs for Scalable Production

IBCs are one of the most effective electrocatalysts for acidic OER. Until now, wet chemistry, sol-gel, laser pulsed, plasma, deposition, and pyrolysis synthesis methods have been applied to synthesize IBCs. Nevertheless, large-scale production is still challenging, which hinders the practical applications of PEMWEs. To increase the production of IBCs, it is necessary to exploit simple and practical synthesis techniques, such as the solid melting method due to its simple preparation procedure and scalability. 3D printing, UV irradiation, possessing facile preparation procedures and large area for placing reactants, should be intensively studied for synthesizing IBCs in industrial production.

Ir is scarce on Earth, which is unfavorable for the future industrial applications. Therefore, developing low-cost high-performance IBCs is an emergency issue that should be solved. More affordable alternative metals should be introduced to boost the industry implementation. Modulation tactics including doping with non-precious metals and loading on non-metal substrates should also be employed to lower the amount of the precious metal Ir used. Moreover, research on increasing the atom utilization efficiency of Ir, such as porous structures and nanocages, should be thoroughly studied to developing more efficient IBCs for acidic OER.

(3) Highly Active and Stable IBCs for Acidic Oxygen Evolution Reaction

Although a series of advanced engineering strategies have been applied to improving the activity and stability of IBCs for acidic oxygen evolution reaction, it is still far from large scale application. From the aspect of enhancing activity, alkali metal and transition metal have been adopted to alloy with Ir to improve the activity. However, the activity of transition metals, such as Fe, Co, Ni, may gradually reduce due to the corrosion of the transition metal ions in harsh acid environment, leading to poor stability. In this scenario, intercalation of other stable elements should be explored to both modify the electronic structures of IBCs and improve the stability in acidic solutions. As for the stability of IBCs, morphology engineering and support engineering have been proposed to optimize the durability of IBCs in acidic OER. Considering the practical harsh working conditions of PEMWEs, IBCs tend to dissolve in the form of Ir (III) and Ir (IV) during the four-electron transfer OER process. Therefore, the durability of the electrocatalyst at high temperature and potential in acidic media should be considered before designation. Supported and novel crystal phase IBCs are considered as the promising stable OER electrocatalysts. Finding support substrates and crystal phase with high electrocatalytic stability and high electrical conductivity are effective approaches to design IBCs with excellent acidic OER performance.

Acknowledgments: The authors would like to thank Australian Research Council (ARC DP200103043) for financial support during this work.

Conflicts of Interest: The authors declare no conflict of interest.

References

1. Seh, Z. W.; Kibsgaard, J.; Dickens, C. F.; Chorkendorff, I.; Nørskov, J. K.; Jaramillo, T. F., Combining theory and experiment in electrocatalysis: Insights into materials design. *Science* **2017,** *355* (6321), eaad4998.
2. Carmo, M.; Fritz, D. L.; Mergel, J.; Stolten, D., A comprehensive review on PEM water electrolysis. *International Journal of Hydrogen Energy* **2013,** *38* (12), 4901-4934.
3. Grubb, W. T.; Niedrach, L. W., Batteries with Solid Ion-Exchange Membrane Electrolytes. *Journal of The Electrochemical Society* **1960,** *107* (2), 131.
4. Song, J.; Wei, C.; Huang, Z.-F.; Liu, C.; Zeng, L.; Wang, X.; Xu, Z. J., A review on fundamentals for designing oxygen evolution electrocatalysts. *Chemical Society Reviews* **2020,** *49* (7), 2196-2214.
5. Wang, Y.; Shen, G.; Zhang, Y.; Pan, L.; Zhang, X.; Zou, J.-J., Visible-light-induced unbalanced charge on NiCoP/TiO_2 sensitized system for rapid H2 generation from hydrolysis of ammonia borane. *Applied Catalysis B: Environmental* **2020,** *260*, 118183.
6. Wang, X.; Zhuang, L.; He, T.; Jia, Y.; Zhang, L.; Yan, X.; Gao, M.; Du, A.; Zhu, Z.; Yao, X.; Yu, S.-H., Grafting Cobalt Diselenide on Defective Graphene for Enhanced Oxygen Evolution Reaction. *iScience* **2018,** *7*, 145-153.
7. Cai, C.; Han, S.; Tang, Y., Engineering oxygen vacancies on dendrite-like IrO_2 for the oxygen evolution reaction in acidic solution. *Sustainable Energy & Fuels* **2020,** *4* (5), 2462-2468.
8. Lim, J.; Park, D.; Jeon, S. S.; Roh, C.-W.; Choi, J.; Yoon, D.; Park, M.; Jung, H.; Lee, H., Ultrathin IrO_2 Nanoneedles for Electrochemical Water Oxidation. *Advanced Functional Materials* **2018,** *28* (4), 1704796.
9. Zhong, W.; Lin, Z.; Feng, S.; Wang, D.; Shen, S.; Zhang, Q.; Gu, L.; Wang, Z.; Fang, B., Improved oxygen evolution activity of IrO_2 by in situ engineering of an ultra-small Ir sphere shell utilizing a pulsed laser. *Nanoscale* **2019,** *11* (10), 4407-4413.
10. Zhang, L.; Lu, C.; Ye, F.; Pang, R.; Liu, Y.; Wu, Z.; Shao, Z.; Sun, Z.; Hu, L., Selenic Acid Etching Assisted Vacancy Engineering for Designing Highly Active Electrocatalysts toward the Oxygen Evolution Reaction. *Advanced Materials* **2021,** *33* (14), 2007523.
11. Deng, Q.; Sun, Y.; Wang, J.; Chang, S.; Ji, M.; Qu, Y.; Zhang, K.; Li, B., Boosting OER performance of IrO_2 in acid via urchin-like hierarchical-structure design. *Dalton Transactions* **2021,** *50* (18), 6083-6087.
12. Chourashiya, M. G.; Urakawa, A., Solution combustion synthesis of highly dispersible and dispersed iridium oxide as an anode catalyst in PEM water electrolysis. *Journal of Materials Chemistry A* **2017,** *5* (10), 4774-4778.
13. Li, G.; Li, S.; Xiao, M.; Ge, J.; Liu, C.; Xing, W., Nanoporous IrO_2 catalyst with enhanced activity and durability for water oxidation owing to its micro/mesoporous structure. *Nanoscale* **2017,** *9* (27), 9291-9298.
14. Zhou, G.; Wang, P.; Hu, B.; Shen, X.; Liu, C.; Tao, W.; Huang, P.; Liu, L., Spin-related symmetry breaking induced by half-disordered hybridization in $Bi_xEr_{2-x}Ru_2O_7$ pyrochlores for acidic oxygen evolution. *Nature Communications* **2022,** *13* (1), 4106.
15. Baik, C.; Lee, S. W.; Pak, C., Control of the pore size distribution inside the RuO_2 catalyst by using silica nanosphere particle for highly efficient water electrolysis. *Microporous and Mesoporous Materials* **2020,** *309*, 110567.
16. Naito, T.; Shinagawa, T.; Nishimoto, T.; Takanabe, K., Recent advances in understanding oxygen evolution reaction mechanisms over iridium oxide. *Inorganic Chemistry Frontiers* **2021,** *8* (11), 2900-2917.
17. Chen, Z.; Guo, L.; Pan, L.; Yan, T.; He, Z.; Li, Y.; Shi, C.; Huang, Z. F.; Zhang, X.; Zou, J. J., Advances in oxygen evolution electrocatalysts for proton exchange membrane water electrolyzers. *Advanced Energy Materials* **2022,** *12* (14), 2103670.
18. Li, L.; Wang, P.; Shao, Q.; Huang, X., Recent progress in advanced electrocatalyst design for acidic oxygen evolution reaction. *Advanced Materials* **2021,** *33* (50), 2004243.
19. He, J.; Zhou, X.; Xu, P.; Sun, J., Regulating Electron Redistribution of Intermetallic Iridium Oxide by Incorporating Ru for Efficient Acidic Water Oxidation. *Advanced Energy Materials* **2021,** *11* (48).
20. Willinger, E.; Massué, C.; Schlögl, R.; Willinger, M. G., Identifying Key Structural Features of IrO_x Water Splitting Catalysts. *Journal of the American Chemical Society* **2017,** *139* (34), 12093-12101.
21. Pi, Y.; Guo, J.; Shao, Q.; Huang, X., Highly Efficient Acidic Oxygen Evolution Electrocatalysis Enabled by Porous Ir–Cu Nanocrystals with Three-Dimensional Electrocatalytic Surfaces. *Chemistry of Materials* **2018,** *30* (23), 8571-8578.
22. Shan, J.; Guo, C.; Zhu, Y.; Chen, S.; Song, L.; Jaroniec, M.; Zheng, Y.; Qiao, S.-Z., Charge-Redistribution-Enhanced Nanocrystalline Ru@IrO_x Electrocatalysts for Oxygen Evolution in Acidic Media. *Chem* **2019,** *5* (2), 445-459.
23. Wu, G.; Zheng, X.; Cui, P.; Jiang, H.; Wang, X.; Qu, Y.; Chen, W.; Lin, Y.; Li, H.; Han, X., A general synthesis approach for amorphous noble metal nanosheets. *Nature communications* **2019,** *10* (1), 1-8.
24. Dang, Q.; Lin, H.; Fan, Z.; Ma, L.; Shao, Q.; Ji, Y.; Zheng, F.; Geng, S.; Yang, S.-Z.; Kong, N.; Zhu, W.; Li, Y.; Liao, F.; Huang, X.; Shao, M., Iridium metallene oxide for acidic oxygen evolution catalysis. *Nature Communications* **2021,** *12* (1), 6007.
25. Fan, Z.; Ji, Y.; Shao, Q.; Geng, S.; Zhu, W.; Liu, Y.; Liao, F.; Hu, Z.; Chang, Y.-C.; Pao, C.-W.; Li, Y.; Kang, Z.; Shao, M., Extraordinary acidic oxygen evolution on new phase 3R-iridium oxide. *Joule* **2021,** *5* (12), 3221-3234.
26. Xu, J.; Lian, Z.; Wei, B.; Li, Y.; Bondarchuk, O.; Zhang, N.; Yu, Z.; Araujo, A.; Amorim, I.; Wang, Z.; Li, B.; Liu, L., Strong Electronic Coupling between Ultrafine Iridium–Ruthenium Nanoclusters and Conductive, Acid-Stable Tellurium Nanoparticle Support for Efficient and Durable Oxygen Evolution in Acidic and Neutral Media. *ACS Catalysis* **2020,** *10* (6), 3571-3579.

27. Shi, Z.; Wang, Y.; Li, J.; Wang, X.; Wang, Y.; Li, Y.; Xu, W.; Jiang, Z.; Liu, C.; Xing, W.; Ge, J., Confined Ir single sites with triggered lattice oxygen redox: Toward boosted and sustained water oxidation catalysis. *Joule* **2021,** *5* (8), 2164-2176.
28. Wu, X.; Feng, B.; Li, W.; Niu, Y.; Yu, Y.; Lu, S.; Zhong, C.; Liu, P.; Tian, Z.; Chen, L.; Hu, W.; Li, C. M., Metal-support interaction boosted electrocatalysis of ultrasmall iridium nanoparticles supported on nitrogen doped graphene for highly efficient water electrolysis in acidic and alkaline media. *Nano Energy* **2019,** *62*, 117-126.
29. Suen, N.-T.; Hung, S.-F.; Quan, Q.; Zhang, N.; Xu, Y.-J.; Chen, H. M., Electrocatalysis for the oxygen evolution reaction: recent development and future perspectives. *Chemical Society Reviews* **2017,** *46* (2), 337-365.
30. Rossmeisl, J.; Qu, Z. W.; Zhu, H.; Kroes, G. J.; Nørskov, J. K., Electrolysis of water on oxide surfaces. *Journal of Electroanalytical Chemistry* **2007,** *607* (1), 83-89.
31. Yu, J.; He, Q.; Yang, G.; Zhou, W.; Shao, Z.; Ni, M., Recent Advances and Prospective in Ruthenium-Based Materials for Electrochemical Water Splitting. *ACS Catalysis* **2019,** *9* (11), 9973-10011.
32. Shan, J.; Zheng, Y.; Shi, B.; Davey, K.; Qiao, S.-Z., Regulating Electrocatalysts via Surface and Interface Engineering for Acidic Water Electrooxidation. *ACS Energy Letters* **2019,** *4* (11), 2719-2730.
33. Wu, H.; Wang, Y.; Shi, Z.; Wang, X.; Yang, J.; Xiao, M.; Ge, J.; Xing, W.; Liu, C., Recent developments of Iridium-based catalysts for oxygen evolution reaction in acidic water electrolysis. *Journal of Materials Chemistry A* **2022**.
34. Nong, H. N.; Reier, T.; Oh, H.-S.; Gliech, M.; Paciok, P.; Vu, T. H. T.; Teschner, D.; Heggen, M.; Petkov, V.; Schlögl, R.; Jones, T.; Strasser, P., A unique oxygen ligand environment facilitates water oxidation in hole-doped IrNiOx core–shell electrocatalysts. *Nature Catalysis* **2018,** *1* (11), 841-851.
35. Chen, Z.; Guo, L.; Pan, L.; Yan, T.; He, Z.; Li, Y.; Shi, C.; Huang, Z. F.; Zhang, X.; Zou, J. J., Advances in Oxygen Evolution Electrocatalysts for Proton Exchange Membrane Water Electrolyzers. *Advanced Energy Materials* **2022,** *12* (14).
36. Zhang, R.; Dubouis, N.; Ben Osman, M.; Yin, W.; Sougrati, M. T.; Corte, D. A. D.; Giaume, D.; Grimaud, A., A Dissolution/Precipitation Equilibrium on the Surface of Iridium-Based Perovskites Controls Their Activity as Oxygen Evolution Reaction Catalysts in Acidic Media. *Angew Chem Int Ed Engl* **2019,** *58* (14), 4571-4575.
37. Kuznetsov, D. A.; Naeem, M. A.; Kumar, P. V.; Abdala, P. M.; Fedorov, A.; Müller, C. R., Tailoring Lattice Oxygen Binding in Ruthenium Pyrochlores to Enhance Oxygen Evolution Activity. *Journal of the American Chemical Society* **2020,** *142* (17), 7883-7888.
38. An, L.; Wei, C.; Lu, M.; Liu, H.; Chen, Y.; Scherer, G. G.; Fisher, A. C.; Xi, P.; Xu, Z. J.; Yan, C. H., Recent development of oxygen evolution electrocatalysts in acidic environment. *Advanced Materials* **2021,** *33* (20), 2006328.
39. Yoo, J. S.; Rong, X.; Liu, Y.; Kolpak, A. M., Role of Lattice Oxygen Participation in Understanding Trends in the Oxygen Evolution Reaction on Perovskites. *ACS Catalysis* **2018,** *8* (5), 4628-4636.
40. Huang, Z.-F.; Song, J.; Du, Y.; Xi, S.; Dou, S.; Nsanzimana, J. M. V.; Wang, C.; Xu, Z. J.; Wang, X., Chemical and structural origin of lattice oxygen oxidation in Co–Zn oxyhydroxide oxygen evolution electrocatalysts. *Nature Energy* **2019,** *4* (4), 329-338.
41. An, L.; Wei, C.; Lu, M.; Liu, H.; Chen, Y.; Scherer, G. G.; Fisher, A. C.; Xi, P.; Xu, Z. J.; Yan, C. H., Recent Development of Oxygen Evolution Electrocatalysts in Acidic Environment. *Adv Mater* **2021,** *33* (20), e2006328.
42. Zagalskaya, A.; Alexandrov, V., Role of Defects in the Interplay between Adsorbate Evolving and Lattice Oxygen Mechanisms of the Oxygen Evolution Reaction in RuO_2 and IrO_2. *ACS Catalysis* **2020,** *10* (6), 3650-3657.
43. Liang, X.; Shi, L.; Liu, Y.; Chen, H.; Si, R.; Yan, W.; Zhang, Q.; Li, G.-D.; Yang, L.; Zou, X., Activating Inert, Nonprecious Perovskites with Iridium Dopants for Efficient Oxygen Evolution Reaction under Acidic Conditions. *Angewandte Chemie International Edition* **2019,** *58* (23), 7631-7635.
44. Retuerto, M.; Pascual, L.; Calle-Vallejo, F.; Ferrer, P.; Gianolio, D.; Pereira, A. G.; García, Á.; Torrero, J.; Fernández-Díaz, M. T.; Bencok, P.; Peña, M. A.; Fierro, J. L. G.; Rojas, S., Na-doped ruthenium perovskite electrocatalysts with improved oxygen evolution activity and durability in acidic media. *Nature Communications* **2019,** *10* (1), 2041.
45. Miao, X.; Zhang, L.; Wu, L.; Hu, Z.; Shi, L.; Zhou, S., Quadruple perovskite ruthenate as a highly efficient catalyst for acidic water oxidation. *Nature Communications* **2019,** *10* (1), 3809.
46. Wu, D.; Kusada, K.; Yoshioka, S.; Yamamoto, T.; Toriyama, T.; Matsumura, S.; Chen, Y.; Seo, O.; Kim, J.; Song, C.; Hiroi, S.; Sakata, O.; Ina, T.; Kawaguchi, S.; Kubota, Y.; Kobayashi, H.; Kitagawa, H., Efficient overall water splitting in acid with anisotropic metal nanosheets. *Nature Communications* **2021,** *12* (1), 1145.
47. Hao, S.; Sheng, H.; Liu, M.; Huang, J.; Zheng, G.; Zhang, F.; Liu, X.; Su, Z.; Hu, J.; Qian, Y.; Zhou, L.; He, Y.; Song, B.; Lei, L.; Zhang, X.; Jin, S., Torsion strained iridium oxide for efficient acidic water oxidation in proton exchange membrane electrolyzers. *Nat Nanotechnol* **2021,** *16* (12), 1371-1377.
48. Pi, Y.; Shao, Q.; Wang, P.; Guo, J.; Huang, X., General Formation of Monodisperse IrM (M = Ni, Co, Fe) Bimetallic Nanoclusters as Bifunctional Electrocatalysts for Acidic Overall Water Splitting. *Advanced Functional Materials* **2017,** *27* (27).
49. Fu, L.; Zeng, X.; Cheng, G.; Luo, W., IrCo Nanodendrite as an Efficient Bifunctional Electrocatalyst for Overall Water Splitting under Acidic Conditions. *ACS Appl Mater Interfaces* **2018,** *10* (30), 24993-24998.
50. Feng, J.; Lv, F.; Zhang, W.; Li, P.; Wang, K.; Yang, C.; Wang, B.; Yang, Y.; Zhou, J.; Lin, F.; Wang, G. C.; Guo, S., Iridium-Based Multimetallic Porous Hollow Nanocrystals for Efficient Overall-Water-Splitting Catalysis. *Advanced Materials* **2017,** *29* (47).
51. Shi, Q.; Zhu, C.; Zhong, H.; Su, D.; Li, N.; Engelhard, M. H.; Xia, H.; Zhang, Q.; Feng, S.; Beckman, S. P.; Du, D.; Lin, Y., Nanovoid Incorporated Ir_xCu Metallic Aerogels for Oxygen Evolution Reaction Catalysis. *ACS Energy Letters* **2018,** *3* (9), 2038-2044.

52. Zhao, F.; Wen, B.; Niu, W.; Chen, Z.; Yan, C.; Selloni, A.; Tully, C. G.; Yang, X.; Koel, B. E., Increasing Iridium Oxide Activity for the Oxygen Evolution Reaction with Hafnium Modification. *J Am Chem Soc* **2021,** *143* (38), 15616-15623.
53. Zheng, Y.-R.; Vernieres, J.; Wang, Z.; Zhang, K.; Hochfilzer, D.; Krempl, K.; Liao, T.-W.; Presel, F.; Altantzis, T.; Fatermans, J.; Scott, S. B.; Secher, N. M.; Moon, C.; Liu, P.; Bals, S.; Van Aert, S.; Cao, A.; Anand, M.; Nørskov, J. K.; Kibsgaard, J.; Chorkendorff, I., Monitoring oxygen production on mass-selected iridium–tantalum oxide electrocatalysts. *Nature Energy* **2021,** *7* (1), 55-64.
54. Wang, Y.; Zhang, L.; Yin, K.; Zhang, J.; Gao, H.; Liu, N.; Peng, Z.; Zhang, Z., Nanoporous Iridium-Based Alloy Nanowires as Highly Efficient Electrocatalysts Toward Acidic Oxygen Evolution Reaction. *ACS Appl Mater Interfaces* **2019,** *11* (43), 39728-39736.
55. Gao, J.; Xu, C. Q.; Hung, S. F.; Liu, W.; Cai, W.; Zeng, Z.; Jia, C.; Chen, H. M.; Xiao, H.; Li, J.; Huang, Y.; Liu, B., Breaking Long-Range Order in Iridium Oxide by Alkali Ion for Efficient Water Oxidation. *J Am Chem Soc* **2019,** *141* (7), 3014-3023.
56. Pi, Y.; Shao, Q.; Zhu, X.; Huang, X., Dynamic Structure Evolution of Composition Segregated Iridium-Nickel Rhombic Dodecahedra toward Efficient Oxygen Evolution Electrocatalysis. *ACS Nano* **2018,** *12* (7), 7371-7379.
57. Wu, G.; Zheng, X.; Cui, P.; Jiang, H.; Wang, X.; Qu, Y.; Chen, W.; Lin, Y.; Li, H.; Han, X.; Hu, Y.; Liu, P.; Zhang, Q.; Ge, J.; Yao, Y.; Sun, R.; Wu, Y.; Gu, L.; Hong, X.; Li, Y., A general synthesis approach for amorphous noble metal nanosheets. *Nat Commun* **2019,** *10* (1), 4855.
58. Yin, J.; Jin, J.; Lu, M.; Huang, B.; Zhang, H.; Peng, Y.; Xi, P.; Yan, C. H., Iridium Single Atoms Coupling with Oxygen Vacancies Boosts Oxygen Evolution Reaction in Acid Media. *J Am Chem Soc* **2020,** *142* (43), 18378-18386.
59. Stamenkovic, V. R.; Mun, B. S.; Arenz, M.; Mayrhofer, K. J. J.; Lucas, C. A.; Wang, G.; Ross, P. N.; Markovic, N. M., Trends in electrocatalysis on extended and nanoscale Pt-bimetallic alloy surfaces. *Nature Materials* **2007,** *6* (3), 241-247.
60. Reier, T.; Pawolek, Z.; Cherevko, S.; Bruns, M.; Jones, T.; Teschner, D.; Selve, S.; Bergmann, A.; Nong, H. N.; Schlogl, R.; Mayrhofer, K. J.; Strasser, P., Molecular Insight in Structure and Activity of Highly Efficient, Low-Ir Ir-Ni Oxide Catalysts for Electrochemical Water Splitting (OER). *J Am Chem Soc* **2015,** *137* (40), 13031-40.
61. Luo, M.; Guo, S., Strain-controlled electrocatalysis on multimetallic nanomaterials. *Nature Reviews Materials* **2017,** *2* (11).
62. Stephens, I. E.; Bondarenko, A. S.; Perez-Alonso, F. J.; Calle-Vallejo, F.; Bech, L.; Johansson, T. P.; Jepsen, A. K.; Frydendal, R.; Knudsen, B. P.; Rossmeisl, J.; Chorkendorff, I., Tuning the activity of Pt(111) for oxygen electroreduction by subsurface alloying. *J Am Chem Soc* **2011,** *133* (14), 5485-91.
63. Calle-Vallejo, F.; Koper, M. T.; Bandarenka, A. S., Tailoring the catalytic activity of electrodes with monolayer amounts of foreign metals. *Chem Soc Rev* **2013,** *42* (12), 5210-30.
64. Pi, Y.; Shao, Q.; Wang, P.; Guo, J.; Huang, X., General Formation of Monodisperse IrM (M = Ni, Co, Fe) Bimetallic Nanoclusters as Bifunctional Electrocatalysts for Acidic Overall Water Splitting. *Advanced Functional Materials* **2017,** *27* (27), 1700886.
65. Fu, L.; Zeng, X.; Cheng, G.; Luo, W., IrCo Nanodendrite as an Efficient Bifunctional Electrocatalyst for Overall Water Splitting under Acidic Conditions. *ACS Applied Materials & Interfaces* **2018,** *10* (30), 24993-24998.
66. Feng, J.; Lv, F.; Zhang, W.; Li, P.; Wang, K.; Yang, C.; Wang, B.; Yang, Y.; Zhou, J.; Lin, F., Iridium-based multimetallic porous hollow nanocrystals for efficient overall-water-splitting catalysis. *Advanced Materials* **2017,** *29* (47), 1703798.
67. Godínez-Salomón, F.; Albiter, L.; Alia, S. M.; Pivovar, B. S.; Camacho-Forero, L. E.; Balbuena, P. B.; Mendoza-Cruz, R.; Arellano-Jimenez, M. J.; Rhodes, C. P., Self-supported hydrous iridium–nickel oxide two-dimensional nanoframes for high activity oxygen evolution electrocatalysts. *ACS Catalysis* **2018,** *8* (11), 10498-10520.
68. Pei, J.; Mao, J.; Liang, X.; Chen, C.; Peng, Q.; Wang, D.; Li, Y., Ir–Cu nanoframes: one-pot synthesis and efficient electrocatalysts for oxygen evolution reaction. *Chemical Communications* **2016,** *52* (19), 3793-3796.
69. Wang, C.; Moghaddam, R. B.; Bergens, S. H., Active, Simple Iridium–Copper Hydrous Oxide Electrocatalysts for Water Oxidation. *The Journal of Physical Chemistry C* **2017,** *121* (10), 5480-5486.
70. Zhao, F.; Wen, B.; Niu, W.; Chen, Z.; Yan, C.; Selloni, A.; Tully, C. G.; Yang, X.; Koel, B. E., Increasing Iridium Oxide Activity for the Oxygen Evolution Reaction with Hafnium Modification. *Journal of the American Chemical Society* **2021,** *143* (38), 15616-15623.
71. Zheng, Y.-R.; Vernieres, J.; Wang, Z.; Zhang, K.; Hochfilzer, D.; Krempl, K.; Liao, T.-W.; Presel, F.; Altantzis, T.; Fatermans, J.; Scott, S. B.; Secher, N. M.; Moon, C.; Liu, P.; Bals, S.; Van Aert, S.; Cao, A.; Anand, M.; Nørskov, J. K.; Kibsgaard, J.; Chorkendorff, I., Monitoring oxygen production on mass-selected iridium–tantalum oxide electrocatalysts. *Nature Energy* **2022,** *7* (1), 55-64.
72. Lv, F.; Feng, J.; Wang, K.; Dou, Z.; Zhang, W.; Zhou, J.; Yang, C.; Luo, M.; Yang, Y.; Li, Y.; Gao, P.; Guo, S., Iridium–Tungsten Alloy Nanodendrites as pH-Universal Water-Splitting Electrocatalysts. *ACS Central Science* **2018,** *4* (9), 1244-1252.
73. Li, R.; Wang, H.; Hu, F.; Chan, K.; Liu, X.; Lu, Z.; Wang, J.; Li, Z.; Zeng, L.; Li, Y., IrW nanochannel support enabling ultrastable electrocatalytic oxygen evolution at 2 A cm^{-2} in acidic media. *Nature communications* **2021,** *12* (1), 1-10.
74. Zhu, J.; Lyu, Z.; Chen, Z.; Xie, M.; Chi, M.; Jin, W.; Xia, Y., Facile Synthesis and Characterization of Pd@Ir_{nL} (n=1–4) Core–Shell Nanocubes for Highly Efficient Oxygen Evolution in Acidic Media. *Chemistry of Materials* **2019,** *31* (15), 5867-5875.
75. Xia, X.; Figueroa-Cosme, L.; Tao, J.; Peng, H.-C.; Niu, G.; Zhu, Y.; Xia, Y., Facile synthesis of iridium nanocrystals with well-controlled facets using seed-mediated growth. *Journal of the American Chemical Society* **2014,** *136* (31), 10878-10881.

76. Xu, J.; Lian, Z.; Wei, B.; Li, Y.; Bondarchuk, O.; Zhang, N.; Yu, Z.; Araujo, A.; Amorim, I.; Wang, Z., Strong electronic coupling between ultrafine iridium–ruthenium nanoclusters and conductive, acid-stable tellurium nanoparticle support for efficient and durable oxygen evolution in acidic and neutral media. *ACS Catalysis* **2020,** *10* (6), 3571-3579.
77. Shan, J.; Ling, T.; Davey, K.; Zheng, Y.; Qiao, S.-Z., Transition-Metal-Doped RuIr Bifunctional Nanocrystals for Overall Water Splitting in Acidic Environments. *Advanced Materials* **2019,** *31* (17), 1900510.
78. Reier, T.; Pawolek, Z.; Cherevko, S.; Bruns, M.; Jones, T.; Teschner, D.; Selve, S.; Bergmann, A.; Nong, H. N.; Schlögl, R.; Mayrhofer, K. J. J.; Strasser, P., Molecular Insight in Structure and Activity of Highly Efficient, Low-Ir Ir–Ni Oxide Catalysts for Electrochemical Water Splitting (OER). *Journal of the American Chemical Society* **2015,** *137* (40), 13031-13040.
79. Massué, C.; Pfeifer, V.; van Gastel, M.; Noack, J.; Algara-Siller, G.; Cap, S.; Schlögl, R., Reactive electrophilic O^{I-} species evidenced in high-performance iridium oxohydroxide water oxidation electrocatalysts. *ChemSusChem* **2017,** *10* (23), 4786-4798.
80. Pfeifer, V.; Jones, T.; Vélez, J. V.; Massué, C.; Greiner, M.; Arrigo, R.; Teschner, D.; Girgsdies, F.; Scherzer, M.; Allan, J., The electronic structure of iridium oxide electrodes active in water splitting. *Physical Chemistry Chemical Physics* **2016,** *18* (4), 2292-2296.
81. Roy, N.; Sohn, Y.; Leung, K. T.; Pradhan, D., Engineered electronic states of transition metal doped TiO_2 nanocrystals for low overpotential oxygen evolution reaction. *The Journal of Physical Chemistry C* **2014,** *118* (51), 29499-29506.
82. Liu, J. X.; Su, H. Y.; Sun, D. P.; Zhang, B. Y.; Li, W. X., Crystallographic dependence of CO activation on cobalt catalysts: HCP versus FCC. *J Am Chem Soc* **2013,** *135* (44), 16284-7.
83. Wang, Y.; Zhang, L.; Yin, K.; Zhang, J.; Gao, H.; Liu, N.; Peng, Z.; Zhang, Z., Nanoporous Iridium-Based Alloy Nanowires as Highly Efficient Electrocatalysts Toward Acidic Oxygen Evolution Reaction. *ACS Applied Materials & Interfaces* **2019,** *11* (43), 39728-39736.
84. Alia, S. M.; Shulda, S.; Ngo, C.; Pylypenko, S.; Pivovar, B. S., Iridium-Based Nanowires as Highly Active, Oxygen Evolution Reaction Electrocatalysts. *ACS Catalysis* **2018,** *8* (3), 2111-2120.
85. Gao, J.; Xu, C.-Q.; Hung, S.-F.; Liu, W.; Cai, W.; Zeng, Z.; Jia, C.; Chen, H. M.; Xiao, H.; Li, J.; Huang, Y.; Liu, B., Breaking Long-Range Order in Iridium Oxide by Alkali Ion for Efficient Water Oxidation. *Journal of the American Chemical Society* **2019,** *141* (7), 3014-3023.
86. Hong, W. T.; Risch, M.; Stoerzinger, K. A.; Grimaud, A.; Suntivich, J.; Shao-Horn, Y., Toward the rational design of non-precious transition metal oxides for oxygen electrocatalysis. *Energy & Environmental Science* **2015,** *8* (5), 1404-1427.
87. Lee, S.; Lee, Y.-J.; Lee, G.; Soon, A., Activated chemical bonds in nanoporous and amorphous iridium oxides favor low overpotential for oxygen evolution reaction. *Nature Communications* **2022,** *13* (1), 3171.
88. Li, W.; Liu, J.; Zhao, D., Mesoporous materials for energy conversion and storage devices. *Nature Reviews Materials* **2016,** *1* (6), 16023.
89. Rashidi, S.; Esfahani, J. A.; Hormozi, F., Classifications of Porous Materials for Energy Applications. In *Encyclopedia of Smart Materials*, 2022; pp 774-785.
90. Yan, X.; Jia, Y.; Yao, X., Defective Structures in Metal Compounds for Energy-Related Electrocatalysis. *Small Structures* **2020,** *2* (2), 2000067.
91. Zhuang, L.; Ge, L.; Yang, Y.; Li, M.; Jia, Y.; Yao, X.; Zhu, Z., Ultrathin Iron-Cobalt Oxide Nanosheets with Abundant Oxygen Vacancies for the Oxygen Evolution Reaction. *Adv Mater* **2017,** *29* (17).
92. Yan, X.; Dong, C.-L.; Huang, Y.-C.; Jia, Y.; Zhang, L.; Shen, S.; Chen, J.; Yao, X., Probing the Active Sites of Carbon-Encapsulated Cobalt Nanoparticles for Oxygen Reduction. *Small Methods* **2019,** *3* (9), 1800439.
93. Tackett, B. M.; Sheng, W.; Kattel, S.; Yao, S.; Yan, B.; Kuttiyiel, K. A.; Wu, Q.; Chen, J. G., Reducing Iridium Loading in Oxygen Evolution Reaction Electrocatalysts Using Core–Shell Particles with Nitride Cores. *ACS Catalysis* **2018,** *8* (3), 2615-2621.
94. Wang, X.; Zhuang, L.; Jia, Y.; Zhang, L.; Yang, Q.; Xu, W.; Yang, D.; Yan, X.; Zhang, L.; Zhu, Z.; Brown, C. L.; Yuan, P.; Yao, X., One-step In-situ Synthesis of Vacancy-rich $CoFe_2O_4$@Defective Graphene Hybrids as Bifunctional Oxygen Electrocatalysts for Rechargeable Zn-Air Batteries. *Chemical Research in Chinese Universities* **2020,** *36* (3), 479-487.
95. Novoselov, K. S.; Geim, A. K.; Morozov, S. V.; Jiang, D.; Zhang, Y.; Dubonos, S. V.; Grigorieva, I. V.; Firsov, A. A., Electric Field Effect in Atomically Thin Carbon Films. *Science* **2004,** *306* (5696), 666-669.
96. Zhang, X.; Lai, Z.; Ma, Q.; Zhang, H., Novel structured transition metal dichalcogenide nanosheets. *Chem Soc Rev* **2018,** *47* (9), 3301-3338.
97. Zu, L.; Qian, X.; Zhao, S.; Liang, Q.; Chen, Y. E.; Liu, M.; Su, B. J.; Wu, K. H.; Qu, L.; Duan, L.; Zhan, H.; Zhang, J. Y.; Li, C.; Li, W.; Juang, J. Y.; Zhu, J.; Li, D.; Yu, A.; Zhao, D., Self-Assembly of Ir-Based Nanosheets with Ordered Interlayer Space for Enhanced Electrocatalytic Water Oxidation. *J Am Chem Soc* **2022,** *144* (5), 2208-2217.
98. Zu, L.; Qian, X.; Zhao, S.; Liang, Q.; Chen, Y.; Su, B.-J.; Wu, K. H.; Qu, L.; Duan, L.; Liu, M.; Zhan, H.; Zhang, J.; Li, C.; Li, W.; Juang, J.-Y.; Zhu, J.; Li, D.; Yu, A.; Zhao, D., Active Origin of Ordered Mesoporous Ir-Based Electrocatalysts for Acidic Water Oxidation. *Joule* **2022**, DOI: 10.2139/ssrn.3900206
99. Liu, J.; Guo, C.; Vasileff, A.; Qiao, S., Nanostructured 2D Materials: Prospective Catalysts for Electrochemical CO_2 Reduction. *Small Methods* **2016,** *1* (1-2).
100. Li, Z.; Zhai, L.; Ge, Y.; Huang, Z.; Shi, Z.; Liu, J.; Zhai, W.; Liang, J.; Zhang, H., Wet-chemical synthesis of two-dimensional metal nanomaterials for electrocatalysis. *National Science Review* **2021,** *9* (5).
101. Jiang, B.; Guo, Y.; Kim, J.; Whitten, A. E.; Wood, K.; Kani, K.; Rowan, A. E.; Henzie, J.; Yamauchi, Y., Mesoporous Metallic Iridium Nanosheets. *Journal of the American Chemical Society* **2018,** *140* (39), 12434-12441.

102. Wu, X.; Feng, B.; Li, W.; Niu, Y.; Yu, Y.; Lu, S.; Zhong, C.; Liu, P.; Tian, Z.; Chen, L., Metal-support interaction boosted electrocatalysis of ultrasmall iridium nanoparticles supported on nitrogen doped graphene for highly efficient water electrolysis in acidic and alkaline media. *Nano Energy* **2019,** *62*, 117-126.
103. Einarsrud, M.-A.; Grande, T., 1D oxide nanostructures from chemical solutions. *Chemical Society Reviews* **2014,** *43* (7), 2187-2199.
104. Xu, C.-Y.; Zhang, Q.; Zhang, H.; Zhen, L.; Tang, J.; Qin, L.-C., Synthesis and characterization of single-crystalline alkali titanate nanowires. *Journal of the American Chemical Society* **2005,** *127* (33), 11584-11585.
105. Zhu, J.; Xie, M.; Chen, Z.; Lyu, Z.; Chi, M.; Jin, W.; Xia, Y., Pt-Ir-Pd trimetallic nanocages as a dual catalyst for efficient oxygen reduction and evolution reactions in acidic media. *Advanced Energy Materials* **2020,** *10* (16), 1904114.
106. Chen, H.; Zhang, M.; Wang, Y.; Sun, K.; Wang, L.; Xie, Z.; Shen, Y.; Han, X.; Yang, L.; Zou, X., Crystal phase engineering of electrocatalysts for energy conversions. *Nano Research* **2022**.
107. Qiao, S.; He, Q.; Zhou, Q.; Zhou, Y.; Xu, W.; Shou, H.; Cao, Y.; Chen, S.; Wu, X.; Song, L., Interfacial electronic interaction enabling exposed Pt(110) facets with high specific activity in hydrogen evolution reaction. *Nano Research* **2022**.
108. Oh, H.-S.; Nong, H. N.; Reier, T.; Bergmann, A.; Gliech, M.; Ferreira de Araújo, J.; Willinger, E.; Schlögl, R.; Teschner, D.; Strasser, P., Electrochemical Catalyst–Support Effects and Their Stabilizing Role for IrO_x Nanoparticle Catalysts during the Oxygen Evolution Reaction. *Journal of the American Chemical Society* **2016,** *138* (38), 12552-12563.
109. Seitz, L. C.; Dickens, C. F.; Nishio, K.; Hikita, Y.; Montoya, J.; Doyle, A.; Kirk, C.; Vojvodic, A.; Hwang, H. Y.; Norskov, J. K., A highly active and stable $IrO_x/SrIrO_3$ catalyst for the oxygen evolution reaction. *Science* **2016,** *353* (6303), 1011-1014.
110. Nong, H. N.; Reier, T.; Oh, H.-S.; Gliech, M.; Paciok, P.; Vu, T. H. T.; Teschner, D.; Heggen, M.; Petkov, V.; Schlögl, R., A unique oxygen ligand environment facilitates water oxidation in hole-doped $IrNiO_x$ core–shell electrocatalysts. *Nature Catalysis* **2018,** *1* (11), 841-851.
111. Wang, L.; Lettenmeier, P.; Golla-Schindler, U.; Gazdzicki, P.; Cañas, N. A.; Morawietz, T.; Hiesgen, R.; Hosseiny, S. S.; Gago, A. S.; Friedrich, K. A., Nanostructured Ir-supported on Ti_4O_7 as a cost-effective anode for proton exchange membrane (PEM) electrolyzers. *Physical Chemistry Chemical Physics* **2016,** *18* (6), 4487-4495.
112. Karimi, F.; Peppley, B. A., Metal carbide and oxide supports for iridium-based oxygen evolution reaction electrocatalysts for polymer-electrolyte-membrane water electrolysis. *Electrochimica Acta* **2017,** *246*, 654-670.
113. Hartig-Weiss, A.; Miller, M.; Beyer, H.; Schmitt, A.; Siebel, A.; Freiberg, A. T.; Gasteiger, H. A.; El-Sayed, H. A., Iridium oxide catalyst supported on antimony-doped tin oxide for high oxygen evolution reaction activity in acidic media. *ACS Applied Nano Materials* **2020,** *3* (3), 2185-2196.
114. Spöri, C.; Kwan, J. T. H.; Bonakdarpour, A.; Wilkinson, D. P.; Strasser, P., The stability challenges of oxygen evolving catalysts: towards a common fundamental understanding and mitigation of catalyst degradation. *Angewandte Chemie International Edition* **2017,** *56* (22), 5994-6021.
115. Geiger, S.; Kasian, O.; Ledendecker, M.; Pizzutilo, E.; Mingers, A. M.; Fu, W. T.; Diaz-Morales, O.; Li, Z.; Oellers, T.; Fruchter, L., The stability number as a metric for electrocatalyst stability benchmarking. *Nature Catalysis* **2018,** *1* (7), 508-515.
116. Li, R.; Wang, H.; Hu, F.; Chan, K. C.; Liu, X.; Lu, Z.; Wang, J.; Li, Z.; Zeng, L.; Li, Y.; Wu, X.; Xiong, Y., IrW nanochannel support enabling ultrastable electrocatalytic oxygen evolution at 2 A cm(-2) in acidic media. *Nature communications* **2021,** *12* (1), 3540.
117. Görlin, M.; Ferreira de Araújo, J.; Schmies, H.; Bernsmeier, D.; Dresp, S.; Gliech, M.; Jusys, Z.; Chernev, P.; Kraehnert, R.; Dau, H.; Strasser, P., Tracking Catalyst Redox States and Reaction Dynamics in Ni–Fe Oxyhydroxide Oxygen Evolution Reaction Electrocatalysts: The Role of Catalyst Support and Electrolyte pH. *Journal of the American Chemical Society* **2017,** *139* (5), 2070-2082.
118. Magkoev, T. T., Formation and Modification of Metal Oxide Substrates for Controlled Molecular Adsorption and Transformation on Their Surface. *Russian Journal of Physical Chemistry A* **2021,** *95* (6), 1081-1092.
119. Yin, J.; Jin, J.; Lu, M.; Huang, B.; Zhang, H.; Peng, Y.; Xi, P.; Yan, C.-H., Iridium Single Atoms Coupling with Oxygen Vacancies Boosts Oxygen Evolution Reaction in Acid Media. *Journal of the American Chemical Society* **2020,** *142* (43), 18378-18386.
120. Nong, H. N.; Oh, H.-S.; Reier, T.; Willinger, E.; Willinger, M.-G.; Petkov, V.; Teschner, D.; Strasser, P., Oxide-Supported $IrNiO_x$ Core–Shell Particles as Efficient, Cost-Effective, and Stable Catalysts for Electrochemical Water Splitting. *Angewandte Chemie International Edition* **2015,** *54* (10), 2975-2979.
121. Nong, H. N.; Gan, L.; Willinger, E.; Teschner, D.; Strasser, P., IrO_x core-shell nanocatalysts for cost-and energy-efficient electrochemical water splitting. *Chemical Science* **2014,** *5* (8), 2955-2963.
122. Böhm, D.; Beetz, M.; Schuster, M.; Peters, K.; Hufnagel, A. G.; Döblinger, M.; Böller, B.; Bein, T.; Fattakhova-Rohlfing, D., Efficient OER Catalyst with Low Ir Volume Density Obtained by Homogeneous Deposition of Iridium Oxide Nanoparticles on Macroporous Antimony-Doped Tin Oxide Support. *Advanced Functional Materials* **2020,** *30* (1), 1906670.
123. Delgado, S.; Lakhtaria, P.; Sousa, E.; Lagarteira, T.; Friedrich, K. A.; Mendes, A., Towards stable and highly active IrO_2 catalysts supported on doped tin oxides for the oxygen evolution reaction in acidic media. *E3S Web Conf.* **2022,** *334*, 03001.
124. Oakton, E.; Lebedev, D.; Povia, M.; Abbott, D. F.; Fabbri, E.; Fedorov, A.; Nachtegaal, M.; Copéret, C.; Schmidt, T. J., IrO_2-TiO_2: A High-Surface-Area, Active, and Stable Electrocatalyst for the Oxygen Evolution Reaction. *ACS Catalysis* **2017,** *7* (4), 2346-2352.
125. Zhuang, L.; Xu, F.; Wang, K.; Li, J.; Liang, C.; Zhou, W.; Xu, Z.; Shao, Z.; Zhu, Z., Porous Structure Engineering of Iridium Oxide Nanoclusters on Atomic Scale for Efficient pH-Universal Overall Water Splitting. *Small* **2021,** *17* (20), e2100121.

 doi:10.20944/preprints202210.0388.v1

126. Luo, F.; Hu, H.; Zhao, X.; Yang, Z.; Zhang, Q.; Xu, J.; Kaneko, T.; Yoshida, Y.; Zhu, C.; Cai, W., Robust and Stable Acidic Overall Water Splitting on Ir Single Atoms. *Nano Lett* **2020,** *20* (3), 2120-2128.
127. Hammer, B.; Norskov, J. K., Why gold is the noblest of all the metals. *Nature* **1995,** *376* (6537), 238-240.
128. Suntivich, J.; May, K. J.; Gasteiger, H. A.; Goodenough, J. B.; Shao-Horn, Y., A perovskite oxide optimized for oxygen evolution catalysis from molecular orbital principles. *Science* **2011,** *334* (6061), 1383-1385.
129. Grimaud, A.; May, K. J.; Carlton, C. E.; Lee, Y.-L.; Risch, M.; Hong, W. T.; Zhou, J.; Shao-Horn, Y., Double perovskites as a family of highly active catalysts for oxygen evolution in alkaline solution. *Nature communications* **2013,** *4* (1), 1-7.
130. Hong, W. T.; Stoerzinger, K. A.; Lee, Y.-L.; Giordano, L.; Grimaud, A.; Johnson, A. M.; Hwang, J.; Crumlin, E. J.; Yang, W.; Shao-Horn, Y., Charge-transfer-energy-dependent oxygen evolution reaction mechanisms for perovskite oxides. *Energy & Environmental Science* **2017,** *10* (10), 2190-2200.
131. Halck, N. B.; Petrykin, V.; Krtil, P.; Rossmeisl, J., Beyond the volcano limitations in electrocatalysis–oxygen evolution reaction. *Physical Chemistry Chemical Physics* **2014,** *16* (27), 13682-13688.